Aza-BODIPY Based Carbonic Anhydrase IX: Strategy to Overcome Hypoxia Limitation in Photodynamic Therapy

Thitima Pewklang,[a] *Kantapat Chansaenpak,*[b] *Rung-Yi Lai,*[a] *Siti Nursyahirah Bakar*[c]*, Chin Siang Kue**[c] *and Anyanee Kamkaew**[a]

[a] School of Chemistry, Institute of Science, Suranaree University of Technology, Nakhon Ratchasima, Thailand 30000

[b] National Nanotechnology Center, National Science and Technology Development Agency, Thailand Science Park, Pathum Thani, Thailand 12120

[c] Faculty of Health and Life Sciences, Management and Science University, Seksyen 13, 40100 Shah Alam, Selangor, Malaysia

KEYWORDS: Aza-BODIPY; PDT; Acetazolamide; hypoxia, Carbonic anhydrase IX

ABSTRACT

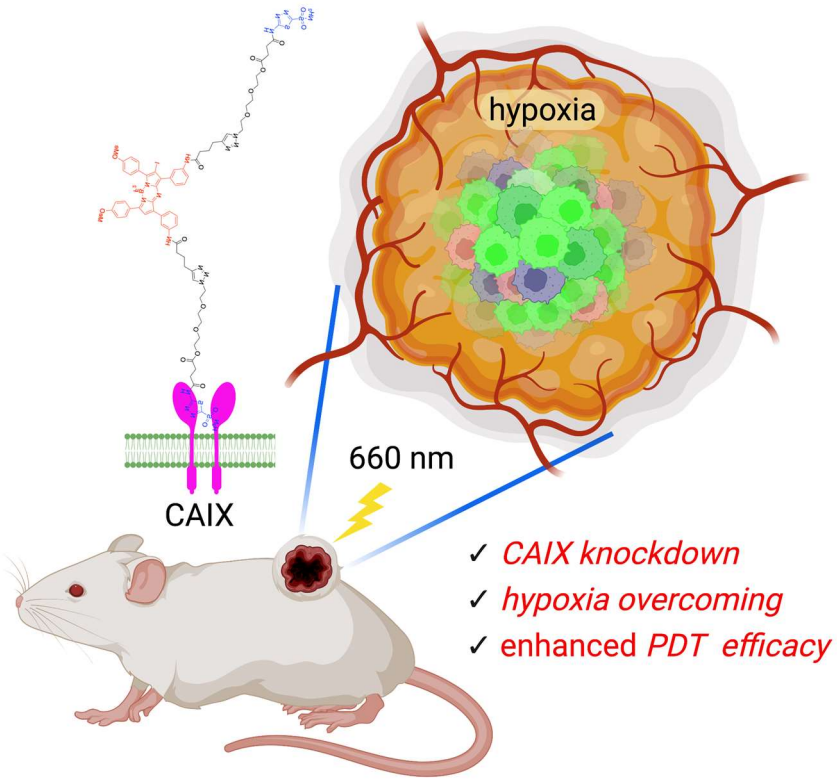

Hypoxia caused by photodynamic therapy (PDT) is a major hurdle to cancer treatment since it can promote recurrence and progression by activating angiogenic factors, lowering therapeutic efficacy dramatically. In this work, **AZB-I-CAIX$_2$** was developed as a carbonic anhydrase IX (CAIX)-targeting NIR photosensitizer that can overcome the challenge by utilizing a combination of CAIX knockdown and PDT. **AZB-I-CAIX$_2$** showed a specific affinity to CAIX-expressed cancer cells and enhanced photocytotoxicity compared to **AZB-I-control** (the molecule without acetazolamide). Moreover, selective detection and effective cell cytotoxicity of **AZB-I-CAIX$_2$** by PDT in hypoxic CAIX-expressed murine cancer cells were achieved. Essentially, **AZB-I-CAIX$_2$** could minimize tumor size in the tumor-bearing mice compared to that in the control groups. The results suggested that **AZB-I-CAIX$_2$** can improve therapeutic efficiency by preventing PDT-induced hypoxia through CAIX inhibition.

Introduction

Photodynamic therapy (PDT) is becoming increasingly popular as a non-invasive cancer treatment in clinical settings. [1, 2] In PDT, a photosensitizer (PS (can be activated by a specific wavelength of light to generate reactive oxygen species R)OS), including singlet oxygen ($^1O_2$) to harm the cells directly through apoptosis and indirectly via tumor vasculature shutdown induction and immune mediators recruitment .[3] Generally, PDT provides more advantages over other conventional cancer treatment approaches including localization improvement, minimally invasive technique, and repeatable without significant side effects.[1, 4] Therefore, PDT provides a safe and effective treatment to selectively clear targeted cells or tissues such as cancer cells while avoiding toxic and side effects on normal or healthy tissues.[5] However, most PDT agents predominantly function through the type II pathway (energy transfer), a highly oxygen -dependent mechanism that can lead to severe tumor hypoxic that the inner region of a tumor has < 20 mmHg O_2 pressure due to insufficient blood supply.[6] PDT-induced hypoxia can restrict the therapeutic effects of PDT and reduce its efficacy in tumor eradication because it triggers the hypoxia-inducing factor (HIF) mediated signaling cascade that upregulates several regulator genes to promote tumor growth.[7] Therefore, developing a PDT system to avoid PDT-induced hypoxia to improve treatments is crucial.

Carbonic anhydrase (CA) has recently been recognized as a valuable target for the development of a variety of diagnostic and therapeutic agents for cancer, due to its overexpression in cancer and as a marker for tumor survival.[8] Lately, it has been shown that two cell surface CA isoforms namely CA IX (almost exclusively associated with tumors) and CA XII (overexpressed in some tumor types) are overexpressed in many tumors and prominently associated with tumor progression.[9] Since many CA isoforms (including CA IX) are linked to anion exchangers or sodium bicarbonate cotransporters, they play an important role in ion transport and electrolyte secretion in a variety of tissues and organs[10]. Hypoxia can regulate the expression of several genes, including those encoding CA IX, through binding of the transcription factor HIF -1 to a hypoxia-responsive element in the gene and is downregulated by the wild-type von Hippel–Lindau tumor

suppressor protein (pVHL).[10, 11] Hypoxia, via the HIF-1 cascade, causes high overexpression of CA IX in many tumors resulting in a pH drop in the tissue. Most hypoxic tumors are acidic (pH =6), while normal tissues are neutral (pH =7.4). Tumor cells decrease their pH_e both by the production of lactic acid (owing to the high glycolysis rate(and by CO_2 hydration catalyzed by the tumor-associated CA IX isoform, which possesses an extracellular catalytic domain [1 2] .Low pH_e has been associated with tumorigenic transformation, chromosomal rearrangements, extracellular matrix breakdown, migration and invasion, induction of cell growth factors, and protease activation [13]. There are some small molecules that could inhibit the catalytic activity of CA. Two major classes of inhibitors that bind to the active site can be distinguished: the inhibitors which coordinate the zinc ion (sulfonamide, sulfamate, sulfamide, dithiocarbamates, xanthate, inorganic anions) and the compounds which do not interact with the metal ion (phenols, polyamines, coumarins).[9] Many potent CA inhibitors derived from acetazolamide, ethoxzolamide, and benzenesulfonamides have been reported to inhibit the growth of several tumor cells *in vitro* and *in vivo* [14] .CAIX-selective sulfonamide inhibitors reduced acidification of the medium, by inhibiting the catalytic activity of the enzyme and thus the generation of H^+ ions, and bound only to hypoxic cells expressing CAIX .Under hypoxic conditions, tumor cells switch on proangiogenic factors such as EGFR and VEGF to promote angiogenesis for regrowth [15] .Therefore, inhibition of CAIX enzymatic activity with targeted PDT conjugate could alleviate hypoxic mediated tumor growth and angiogenesis.[16]

In this study, we used an aza-BODIPY photosensitizer in combination with CA pan-inhibitor, acetazolamide (AZ), to reprogram the hypoxic metabolism that aimed to overcome oxygen deficiency in PDT. Figure 1 shows the structures of the targeting probe and the control in this work. Aza-BODIPY dye could be an ideal PDT agent because it can absorb light in the near IR region since PDT can be more effective if near-IR absorbing photosensitizers (λ_{max} > 700 nm) are used to treat deep-seated tissue.[17] Moreover, their structures are synthetic accessible to conjugate with many targeting ligands.[18, 19, 20] Because the bivalent ligand was shown to have superior selectivity to CAIX,[21] we attached two AZ moieties to the

photosensitizer for our targeting probe. Furthermore, when compared to parent acetazolamide, increasing the tail of AZ resulted in improved Ki over hCA IX.[22] Moreover, the linker was used in the conjugation to improve the compound's binding affinity and hydrophilicity.

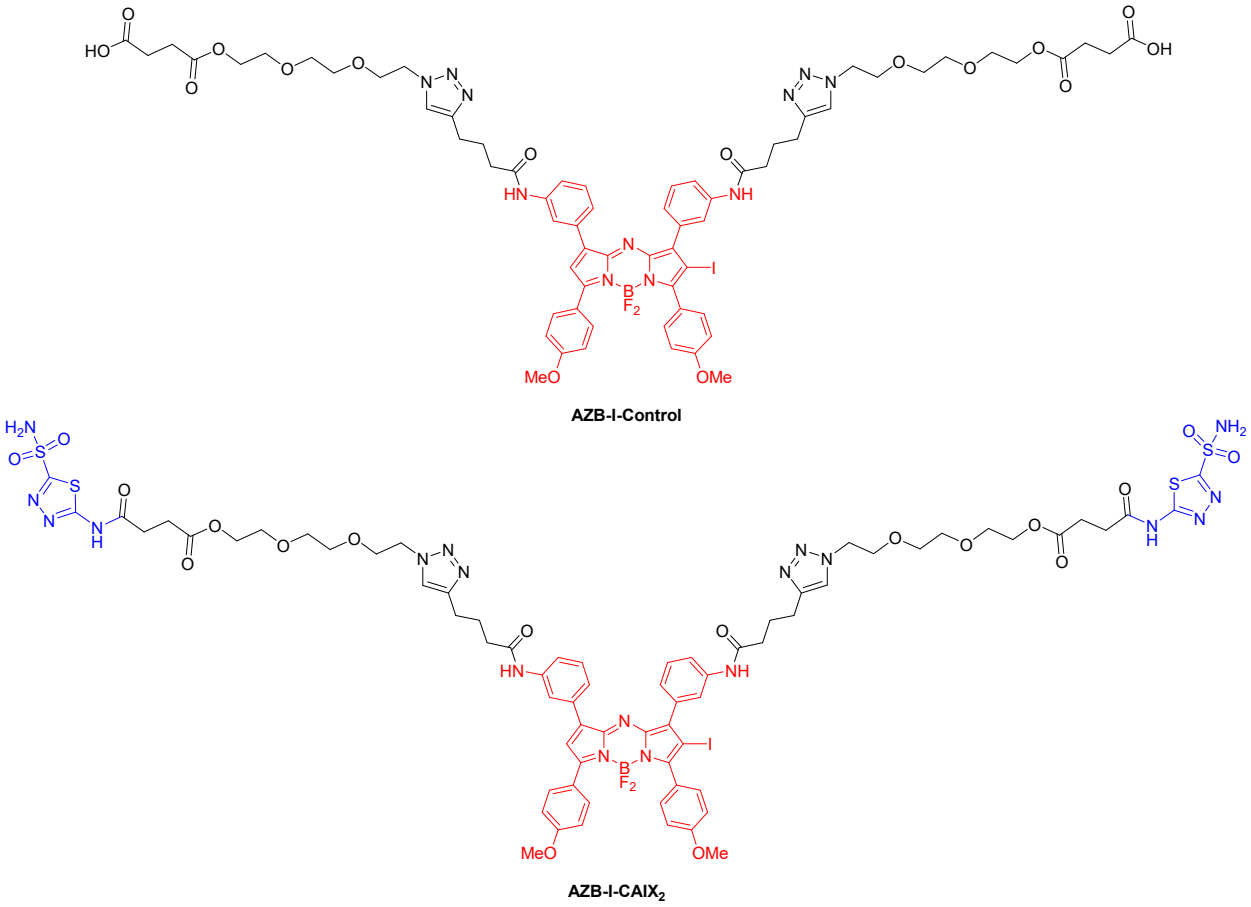

Figure 1. Structures of targeting probe (**AZB-I-CAIX$_2$**) and control (**AZB-I-control**) in this study.

Experimental Section

Chemistry experimental Instruments and synthesis

For all reactions, glassware was oven-dried before use. All the reagents have been purchased from commercial sources and used without further purification. ^{1}H, ^{13}C, and ^{19}F NMR spectra were recorded on a Bruker-500 MHz spectrometer at room temperature. Chemical shifts (δ, ppm) of ^{1}H NMR spectra were reported in $CDCl_3$, MeOD-d_4, and DMSO-d_6 and coupling constant (J, Hz). Mass spectra (MS) were measured under high-resolution ESI conditions. All the UV/vis absorption spectra and fluorescence were recorded on UV-vis Spectrophotometer (Agilent Technologies Cary 300) and Spectrofluorometer (PerkinElmer LS55), respectively. All compounds are > 95% pure by HPLC analysis. Reverse phase HPLC was performed on an Agilent HPLC 1100 and ZORBAX Eclipse XDB-C18 (4.6 mm × 150 mm, 5 μm ID) column using a mobile phase of solvent A = 20 mM ammonium acetate, solvent B = 100 % acetonitrile, isocratic 50 % A: B, and flow rate 1 mL/min. The analysis was monitored by a UV-Vis detector at a wavelength of 280 nm.

4-(2-(2-(2-azidoethoxy)ethoxy)ethoxy)-4-oxobutanoic acid (1).

To solution of **azido-PEG** (1.1848 g, 6.7666 mmol) and succinic anhydride (3.0340 g, 30.319 mmol) in dry DMF (5 mL). Then, the mixture was stirred at 55 ºC for 24 h. After that, the reaction was extracted with dichloromethane and DI water (3 × 100 mL) and followed by brine (100 mL). The organic layer was dried by anhydrous Na_2SO_4 and the solvent was removed under vacuum pressure. The product was obtained without purification to yield 1.8616 g (100 %) of **1** as a pale-yellow oil. ^{1}H NMR (500 MHz, DMSO-d_6): δ = 12.20 (s, 1H), 4.21 (t, J = 5.0 Hz, 2H), 3.69 (t, J = 5.0 Hz, 2H), 3.64 (m, 2H), 3.46 (t, J = 5.0 Hz, 2H), 2.97 (s, 2H), 2.81 (s, 2H), 2.58 (m, 2H), 2.55 (m, 2H). ^{13}C NMR (125 MHz, DMSO-d_6): δ = 174.0, 172.6, 70.3, 70.1, 69.4, 68.8, 63.8, 50.5, 31.2, 29.2 ppm. MS (high resolution ESI^+) m/z: the calculated value (calcd) for $C_{10}H_{17}N_3NaO_6$ ($[M+Na]^+$) : 298.1015, found 298.1010.

2-(2-(2-azidoethoxy)ethoxy)ethyl 4-oxo-4-((5-sulfamoyl-1,3,4-thiadiazol-2-yl)amino)

butanoate (2).

1 (1.5611 g, 5.6744 mmol) and **hydrolyzed acetazolamide** (1.1235 g, 6.2417 mmol) were dissolved in dry DMF (5 mL). The reaction mixture was then cooled to 0 ºC. 1-Ethyl-3-(3-dimethylaminopropyl)carbodiimide (EDC, 1.6317 g, 8.5117 mmol) and 4-dimethylaminopyridine (DMAP, 0.1386, 1.134 mmol) were added into the mixture at 0 °C. The reaction mixture was warm up to 30 ºC and stirred for 24 h. After that, the reaction was extracted with HCl (0.2 N, 1 x 100 mL), DI water (2 x 100 mL) and brine (1 x 100 mL), respectively. The organic layer was then dried over anhydrous Na_2SO_4 and the solvent was removed under reduced pressure. The obtained residue was purified by silica chromatography eluting with hexane: ethyl acetate (3 : 1 to 2 : 1) to yield 1.2897 g (52 %) of **2** as a pale yellow oil. ^{1}H NMR (500 MHz, DMSO-d_6): δ = 8.09 (s, 2H), 7.00 (s, 1H), 4.32 (t, *J* = 5.0 Hz, 2H), 3.78 (t, *J* = 5.0 Hz, 2H), 3.74 (m, 2H), 3.47 (t, *J* = 5.0 Hz, 2H), 3.04 (s, 1H), 3.00 (t, *J* = 7.0 Hz, 2H), 2.95 (s, 1H), 2.86 (t, *J* = 7.0 Hz, 2H). ^{13}C NMR (125 MHz, DMSO-d_6): δ = 172.8, 171.0, 164.4, 162.9, 70.5, 70.4, 69.9, 69.0, 64.2, 50.7 ppm. MS (high resolution ESI$^+$) m/z: the calculated value (calcd) for $C_{12}H_{19}N_7NaO_7S_2$ ([M+Na]$^+$) : 460.0685, found 460.0680.

***N,N′*-((5,5-difluoro-3,7-bis(4-methoxyphenyl)-5H-4l4,5l4-dipyrrolo[1,2-c:2',1'-f][1,3,5,2]triazaborinine-1,9-diyl)bis(3,1-phenylene))bis(hex-5-ynamide) (3).**

AZB-NH$_2$ (0.2040 g, 0.3468 mmol) and **5-hexynoic acid** (0.20 mL, ρ = 1.03, 1.8 mmol) were dissolved in dry dichloromethane (6 mL). The reaction mixture was then cooled to 0 ºC. 1-Ethyl-3-(3-dimethylaminopropyl)carbodiimide (EDC, 0.2600 g, 1.3563 mmol) and 4-dimethylaminopyridine (DMAP, 0.0350 g, 0.0286 mmol) were added into the mixture at 0 °C. The reaction mixture was warm up to 30 ºC and stirred for 2 h. After that, the reaction was extracted with DI water (3 x 100 mL) and brine (1 x 100 mL), respectively. The organic layer was then dried over anhydrous Na_2SO_4 and the solvent was removed under reduced pressure. The obtained residue was purified by silica chromatography eluting with dichloromethane: MeOH (100: 0 to 98 : 2) to yield 0.1972 g (73 %) of **3** as a red metallic solid. ^{1}H NMR (500 MHz, $CDCl_3$ + 3 drops of MeOD-d_4): δ = 7.97 (d, *J* = 9.0 Hz, 2H), 7.95 (s, 1H), 7.67 (s, 1H), 7.66 (s, 1H), 7.28 (t, *J* = 6.0 Hz, 1H), 6.95 (s, 1H), 6.92 (d, *J* = 9.0 Hz, 2H), 3.82 (s, 1H), 2.39 (t, *J* = 7.5 Hz, 2H),

2.25 (t, J = 7.5 Hz, 2H), 1.97 (s, 1H), 1.85 (t, J = 7.5 Hz, 2H). ^{13}C NMR (125 MHz, $CDCl_3$ + 3 drops of MeOD-d_4): δ = 171.4, 162.0, 145.2, 142.3, 138.4, 133.0, 131.7, 129.0, 125.0, 123.9, 120.7, 119.0, 114.9, 83.6, 69.3, 55.4, 35.7, 24.0, 17.9 ppm. MS (high resolution ESI$^+$) m/z: the calculated value (calcd) for $C_{46}H_{40}BF_2N_5NaO_4$ ([M+Na]$^+$) : 798.3039, found 798.3041.

N,N'-((5,5-difluoro-2-iodo-3,7-bis(4-methoxyphenyl)-5H-5l4,6l4-dipyrrolo[1,2-c:2',1'-f][1,3,5,2]triazaborinine-1,9-diyl)bis(3,1-phenylene))bis(hex-5-ynamide) (4).

3 (97.7 mg, 0.1260 mmol) was dissolved in 6 mL of $CHCl_3$: CH_3COOH (3:1). *N*-iodosuccinimide (NIS, 63.2 mg, 0.281 mmol) was then added to the solution and stirred at 30 ^oC for 1 h. After that, the reaction was stopped by adding DI water (20 mL) and extracted with sat. Na_2SO_3 (2 x 20 mL), sat. $NaHCO_3$ (2 x 20 mL) and brine (1 x 100 mL), respectively. The organic layer was then dried over anhydrous Na_2SO_4 and the solvent was removed under reduced pressure. The obtained residue was purified by silica chromatography eluting with 100% dichloromethane to yield 54.5 mg (48 %) of **4** as a red metallic solid. ^{1}H NMR (500 MHz, DMSO-d_6): δ = 10.21 (s, 1H), 10.07 (s, 1H), 8.27 (d, J = 9.0 Hz, 2H), 8.24 (s, 1H), 8.17 (s, 1H), 7.93 (d, J = 8.0 Hz, 1H), 7.80 (d, J = 7.5 Hz, 1H), 7.72 (m, 2H), 7.69 (s, 1H), 7.67 (s, 1H), 7.53 (m, 1H), 7.51 (m, 1H), 7.38 (t, J = 7.5 Hz, 1H), 7.21 (d, J = 9.0 Hz, 2H), 7.18 (d, J = 9.0 Hz, 2H), 3.95 (s, 3H), 3.94 (s, 3H), 2.91 (d, J = 8.5 Hz, 2H), 2.55 (m, 2H), 2.33 (d, J = 7.5 Hz, 2H), 1.87 (dd, J = 7.0, 5.0 Hz, 2H). ^{13}C NMR (125 MHz, DMSO-d_6): δ = 207.3, 171.2, 163.7. 162.4, 161.0, 155.8, 146.8, 145.6, 143.8, 142.9, 139.9, 139.6, 133.3, 133.2, 132.7, 131.8, 129.3, 128.8, 126.1, 125.2, 124.2, 122.6, 122.1, 121.9, 121.1, 120.4, 119.9, 115.2, 113.8, 84.5, 72.1, 56.2, 55.8, 35.5, 24.4, 17.9 ppm, ^{19}F NMR (470 MHz, DMSO-d_6): δ = -131.23 (q, J = 33.0 Hz, BF_2) ppm. MS (high resolution ESI$^+$) m/z: the calculated value (calcd) for $C_{46}H_{39}BF_2IN_5NaO_4$ ([M+Na]$^+$) : 924.2006, found 924.2008.

4,4'-((((((((((5,5-difluoro-2-iodo-3,7-bis(4-methoxyphenyl)-5H-5l4,6l4-dipyrrolo[1,2-c:2',1'-f][1,3,5,2]triazaborinine-1,9-diyl)bis(3,1-phenylene))bis(azanediyl))bis(4-oxobutane-4,1-diyl))bis(1H-1,2,3-triazole-4,1-diyl))bis(ethane-2,1-diyl))bis(oxy))bis(ethane-2,1-diyl))bis(oxy))bis(ethane-2,1-diyl))bis(oxy))bis(4-oxobutanoic acid) (AZB-I-Control)

4 (28.7 mg, 0.0318 mmol) and **1** (38.4 mg, 0.140 mmol) were dissolved in DMSO (0.5 mL). To the reaction mixture was added freshly prepared Na ascorbate solution (1.5 mg in 20 μL of DI water, 7.6 μmol) and freshly prepared $CuSO_4$•$5H_2O$ solution (1.0 mg in 20 μL of DI water, 4.0 μmol), respectively. The resulting mixture was stirred vigorously at 30 ºC for 1 h. After that, the reaction was stopped and precipitated by adding DI water (20 mL). Then, the product was obtained by centrifugation (5000 rpm for 10 min) and washed with DI water (20 mL) for 5 times. The product was obtained without purification to yield 28.1 mg (61 %) of **AZB-I-Control** as a dark green solid. ^{1}H NMR (500 MHz, DMSO-d_6): δ = 12.28 (s, 2H), 10.18 (s, 1H), 10.04 (s, 1H), 8.27 (d, *J* = 8.5 Hz, 2H), 8.25 (s, 1H), 8.17 (s, 1H), 7.94 (s, 1H), 7.92 (s, 1H), 7.89 (s, 1H), 7.79 (d, *J* = 8.0 Hz, 1H), 7.71 (s, 1H), 7.68 (d, *J* = 8.5 Hz, 2H), 7.53 (m, 1H), 7.50 (m, 1H), 7.36 (t, *J* = 7.5 Hz, 1H), 7.21 (d, *J* = 8.5 Hz, 2H), 7.18 (d, *J* = 8.5 Hz, 2H), 4.54 (m, 4H), 4.17 (m, 4H), 3.96 (s, 3H), 3.95 (s, 3H), 3.87 (m, 4H), 3.62 (m, 4H), 3.59 (m, 4H), 3.57 (m, 4H), 2.77 (m, 4H), 2.54 (m, 4H), 2.53 (m, 4H), 2.51 (m, 4H), 2.00 (m, 4H). ^{13}C NMR (125 MHz, DMSO-d_6): δ = 173.8, 172.6, 171.6, 163.7, 162.4, 161.0, 155.8, 146.8, 145.6, 143.9, 142.9, 140.0, 139.7, 133.3, 133.2, 132.7, 131.8, 129.3, 128.8, 126.1, 125.2, 124.2, 122.8, 122.6, 122.1, 121.8, 121.1, 120.4, 119.8, 115.4, 115.2, 113.8, 70.1, 70.0, 69.2, 68.7, 63.8, 56.2, 55.8, 49.9, 36.3, 36.2, 29.1, 25.4, 25.3, 25.1 ppm, ^{19}F NMR (470 MHz, DMSO-d_6): δ = -131.23 (q, *J* = 33.0 Hz, BF_2) ppm. MS (high resolution ESI$^+$) m/z: the calculated value (calcd) for $C_{66}H_{73}BF_2IN_{11}O_{16}$ ($[M]^+$): 1451.4343, found 1451.4348. The compound was 98 % pure by HPLC analysis with retention time 3.59 min (Figure S1).

2-(2-(2-(4-(4-((3-(5,5-difluoro-2-iodo-3,7-bis(4-methoxyphenyl)-9-(3-(4-(1-(2-(2-(2-((4-oxo-4-((5-sulfamoyl-1,3,4-thiadiazol-2-yl)amino)butanoyl)oxy)ethoxy)ethoxy)ethyl)-1H-1,2,3-triazol-4-yl)butanamido)phenyl)-5H-5l4,6l4-dipyrrolo[1,2-c:2',1'-f][1,3,5,2]triazaborinin-1-yl)phenyl)amino)-4-oxobutyl)-1H-1,2,3-triazol-1-yl)ethoxy)ethoxy)ethyl 4-oxo-4-((5-sulfamoyl-1,3,4-thiadiazol-2-yl)amino)butanoate (AZB-I-CAIX$_2$)

4 (40.0 mg, 0.0444 mmol) and **2** (60.8 mg, 0.139 mmol) were dissolved in DMSO (0.5 mL). To the reaction mixture was added freshly prepared Na ascorbate solution (3.0 mg in 20 μL of DI water, 15 μmol) and freshly prepared $CuSO_4•5H_2O$ solution (2.0 mg in 20 μL of DI water, 8.0 μmol), respectively. The resulting mixture was stirred vigorously at 30 ºC for 1 h. After that, the reaction was stopped and precipitated by adding DI water (20 mL). Then, the product was obtained by centrifugation (5000 rpm for 10 min) and washed with DI water (20 mL) for 5 times. The product was obtained without purification to yield 48.4 mg (61 %) of **AZB-I-CAIX$_2$** as a dark green solid. ^{1}H NMR (500 MHz, DMSO-d_6): δ = 10.07 (s, 1H), 9.93 (s, 1H), 8.30 (s, 4H), 8.19 (d, *J* = 8.5 Hz, 2H), 8.16 (s, 1H), 8.09 (s, 1H), 7.86 (m, 1H), 7.85 (m, 1H), 7.84 (m, 1H), 7.70 (d, *J* = 7.5 Hz, 2H), 7.62 (s, 1H), 7.60 (d, *J* = 8.5 Hz, 2H), 7.45 (m, 1H), 7.42 (m, 1H), 7.29 (t, *J* = 7.5 Hz, 1H), 7.13 (d, *J* = 8.5 Hz, 2H), 7.10 (d, *J* = 8.5 Hz, 2H), 4.46 (t, *J* = 6.0 Hz, 4H), 4.09 (t, *J* = 4.0 Hz, 4H), 3.88 (s, 3H), 3.87 (s, 3H), 3.79 (t, *J* = 6.0 Hz, 4H), 3.54 (t, *J* = 4.0 Hz, 4H), 3.49 (m, 4H), 3.48 (m, 4H), 2.80 (m, 4H), 2.69 (m, 4H), 2.68 (t, *J* = 6.5 Hz, 4H), 2.42 (m, 4H), 1.94 (m, 4H). ^{13}C NMR (125 MHz, DMSO-d_6): δ = 171.6, 171.5, 171.4, 171.2, 171.1, 163.7, 152.4, 161.0, 155.9, 146.8, 145.6, 142.9, 140.0, 139.6, 133.3, 133.2, 132.7, 131.8, 129.3, 128.8, 126.1, 125.2, 124.3, 122.7, 122.6, 122.1, 121.9, 121.1, 120.4, 120.0, 115.2, 114.9, 113.8, 72.8, 72.1, 70.1, 69.2, 60.7, 56.2, 55.8, 49.7, 36.3, 35.6, 25.4, 25.1, 24.4, 17.9 ppm. MS (high resolution ESI$^+$) m/z: the calculated value (calcd) for $C_{70}H_{76}BF_2IN_{19}O_{18}S_4$ ([M-H]$^-$): 1774.3599, found 1774.3587. The compound was 96 % pure by HPLC analysis with retention time 11.51 min (Figure S1).

Fluorescent Quantum Yields (Φ_f)

The UV/vis absorption spectra and fluorescence were recorded on UV-vis Spectrophotometer (Agilent Technologies Cary 300) and Spectrofluorometer (PerkinElmer LS55), respectively. Briefly, **AZB-I-CAIX$_2$** and **AZB-I-Control** are stocked in DMSO. The stock solution of **AZB-I-CAIX$_2$** and **AZB-I-Control** were added to quartz cell of 1 cm path length in various solvents ($CHCl_3$, DMSO, MeOH, and

PBS 3% tween 80) to a final concentration of 1 μM. The fluorescence spectra used the following parameters of excitation wavelengths at 670 nm. The fluorescence quantum yields were calculated using equation (1).

$$\Phi_f = \Phi_{std}\left(\frac{A_{sample}}{A_{std}}\right)\left(\frac{I_{std}}{I_{sample}}\right)\left(\frac{\eta_{sample}}{\eta_{std}}\right)^2 \quad (1)$$

where Φ_{std} denotes the fluorescence quantum yield of standard Zn-phthalocyanine in pyridine, A is the peak area of emission, I is the absorbance at the excitation wavelength, and ŋ stands for the solvent reflective index.

Singlet Oxygen Quantum Yields (Φ_Δ)

Singlet oxygen Quantum Yields of **AZB-I-CAIX₂** and **AZB-I-Control** were determined using a red LED lamp (660 nm, power density of 8.7 mW cm^{-2}) in DMSO at room temperature compared to a standard singlet oxygen probe (methylene blue). A solution of DMSO containing 50 μM of 1,3-diphenylisobenzofuran (DPBF, TCI) as a singlet oxygen scavenger and 0.5 μM of **AZB-I-CAIX₂** in a quartz cell of 1 cm path length. The DPBF solution in DMSO (negative control), the solution containing 0.5 μM of **AZB-I-Control,** and the solution containing 0.5 μM methylene blue (comparative control) were also examined. After being exposed to the lamp, the absorbance reduction of DPBF at 408 nm was measured during 0-60 s by an Agilent UV-Vis spectrophotometer (carry 300). The changing of absorbance is plotted against irradiation time. The singlet oxygen quantum yield was calculated according to equation (2).

$$\Phi_\Delta = \Phi_{std}\left(\frac{grad_{sample}}{grad_{std}}\right)\left(\frac{F_{std}}{F_{sample}}\right) \quad (2)$$

Where Φ_{std} denotes the singlet oxygen quantum yield of methylene blue (0.52 in DMSO), grad is the rate of reaction, and F is the absorption correction factor ($F = 1–10^{-absorbance}$).

Biological studies experiments

1. Cell cultures

For human cell lines, CAIX expression in MDA-MB-231 (human breast cancer) is significantly higher than in other cell lines including MCF-7 (human breast cancer), HeLa (human cervical cancer), A549 (human lung cancer), and HEK-293 (human embryonic kidney). Therefore, those cell lines are performed using different endogenous CAIX expression levels. MDA-MB-231, MCF-7, HeLa, and Hek293 were cultured in Dulbecco's Modified Eagle's Media (DMEM, Gibco) and A549 in Kaighn's Modification of Ham's F-12 Medium (F-12K, ATCC). For murine cell lines, 4T1 (murine mammary carcinoma) is higher CAIX expression than 67NR (mouse breast cancer). Two murine cell lines were cultured in RPMI (Gibco). All cell lines were cultured on 75 cm^3 cell culture flasks (NEST) supplemented with 10% fetal bovine serum (FBS, Hyclone) and 1% penicillin-streptomycin (P/S, Corning) under humidified 95% air, 5% CO_2 atmosphere at 37 ^oC.

2. Time and dose dependent cellular uptake in human cell lines

All human cell lines (MDA-MB-231, MCF-7, HeLa, A549, and Hek293) were seeded on 8-well (LabTek II Chamber Slide x/Cover RS Glass Slide Sterile) at 1 x 10^4/well and incubated at 37 ^oC for 24 h. After that, the cells were incubated with 5 μM of **AZB-I-CAIX$_2$** (all cells) and **AZB-I-Control** (MDA-MB-231 and MCF-7) for 0, 1, 3, 6, and 24 h. For dose dependent experiment, MDA-MB-231 cells were incubated with 0, 1, 2.5, and 5 μM of **AZB-I-CAIX$_2$** for 0, 6 h. Then, the cells were washed three times with 0.01 M of PBS buffer (pH 7.4) and treated with media containing 1.0 μM Hoechst 33342 (DNA fluorescent staining, Thermo Fisher Scientific) for 10 min. The cells were visualized under 60X oil immersion objective lens by Laser Scanning Confocal Microscope (Nikon A1Rsi) with 561 nm laser (**AZB-I-CAIX$_2$** and **AZB-I-Control**) and 405 nm laser (Hoechst33342). Quantitative corrected total cell fluorescence data was quantified using ImageJ and represented the mean ± SD (n = 50). Statistical analysis: One-way ANOVA followed by Tukey's analysis was used for comparison between multiple groups using

GraphPad Prism9 software. P values of less than 0.05 (95% confidence interval) are considered significant (ns $p < 0.12$, * $p < 0.033$, ** $p < 0.002$, *** $p < 0.001$).

3. Co-cultured between (+) and (-) CAIX expression cell lines

Positive CAIX expression cell (MDA-MB-231) and negative CAIX expression cell (MCF-7) were seeded on 35-mm glass-bottom confocal dishes (NEST) at 2 x 10^5/well in single media and incubated at 37 ^oC for 24 h. After that, the cells were incubated with 5 μM of **AZB-I-CAIX$_2$** for 6 h. Then, the cells were washed three times with 0.01 M of PBS buffer (pH 7.4) and treated with media containing 1.0 μM Hoechst33342 for 10 min. The cells were visualized under 60X oil immersion objective lens by Laser Scanning Confocal Microscope (Nikon A1Rsi) with 561 nm laser (**AZB-I-CAIX$_2$**) and 405 nm laser (Hoechst33342).

4. Competitive effect with CAIX ligand

Positive CAIX expression cell lines (MDA-MB-231) were seeded on 8-well (LabTek II Chamber Slide x/Cover RS Glass Slide Sterile) at 1 x 10^4/well and incubated at 37 ^oC for 24 h. After that, the cells were incubated with 5 μM of **AZB-I-CAIX$_2$** and 0, 5, 50, 100, 500, and 1000 μM of acetazolamide (CAIX ligand) for 6 h. For time-dependent competition effect with CAIX inhibitor, MDA-MB-231 cells were incubated with 5 μM of **AZB-I-CAIX$_2$** and 500 μM of acetazolamide for 0, 1, 3, and 6 h. Then, the cells were washed three times with 0.01 M of PBS buffer (pH 7.4) and treated with media containing 1.0 μM Hoechst33342 for 10 min. The cells were visualized under 60X oil immersion objective lens by Laser Scanning Confocal Microscope (Nikon A1Rsi) with 561 nm laser (**AZB-I-CAIX$_2$**) and 405 nm laser (Hoechst33342). Quantitative corrected total cell fluorescence data was quantified using ImageJ and represented the mean ± SD (n = 50). Statistical analysis: t-test followed by Tukey's analysis was used for comparison between multiple groups using GraphPad Prism9 software. P values of less than 0.05 (95% confidence interval) are considered significant (ns $p < 0.12$, * $p < 0.033$, ** $p < 0.002$, *** $p < 0.001$).

5. Colocalization study

Positive CAIX expression cell lines (MDA-MB-231) were seeded on 8-well (LabTek II Chamber Slide x/Cover RS Glass Slide Sterile) at 1 x 10^4/well and incubated at 37 ºC for 24 h. After that, the cells were incubated with 5 μM of **AZB-I-CAIX$_2$** for 6 h. Then, the cells were washed three times with 0.01 M of PBS buffer (pH 7.4) and treated with 1.0 μM Hoechst33342 in media containing 1.0 μM of MitoTracker™ Green FM (Thermo Fisher Scientific), LysoTracker™ Green DND-26 (Thermo Fisher Scientific), C6-NBD Ceramide (Golgi tracker, Avanti Polar Lipids), and ER-Tracker™ Green (BODIPY™ FL Glibenclamide, Thermo Fisher Scientific) for 20 min. The cells were visualized under 60X oil immersion objective lens by Laser Scanning Confocal Microscope (Nikon A1Rsi) with 641 nm laser (**AZB-I-CAIX$_2$**), 488 nm laser (Mitotracker, Lysotracker, Golgitracker, and ERtracker), and 405 nm laser (Hoechst33342). Pearson's correlation coefficient for colocalization of **AZB-I-CAIX$_2$** and organelles trackers were obtained from ImageJ

6. Cell cytotoxicity assay

All human cell lines (MDA-MB-231, MCF-7, HeLa, A549, and Hek293) were seeded on a 96-well cell culture plate at approximately 7 × 10^3 cells per well for 24 h. After that, the cells were incubated with 0, 0.125, 0.25, 0.5, 1, 2, 5, and 10 μM of **AZB-I-CAIX$_2$** (all cells) and **AZB-I-Control** (MDA-MB-231 and MCF-7) for 6 h. After incubation, the cells were washed with 0.01 M of PBS pH 7.4 (3 times) before being irradiated by a red LED lamp (660 nm, power density of 8.7 mW cm^{-2}) for 0, 5, 10, and 15 min, and then re-incubated for another 24 h. Then, the cells were added with 0.5 mg mL^{-1} of MTT reagent (Methylthiazolyldiphenyl-tetrazolium bromide, Sigma-Aldrich) in 0.01 M PBS (pH 7.4) solution for 2.5 h. After the solution of MTT reagent removal, the formazan product was dissolved by adding DMSO. The cell cytotoxicity was detected through UV-vis absorption of formazan at wavelength 560 nm using a microplate reader (BMG Labtech/SPECTROstar Nano). IC_{50} values of cell viability were evaluated by GraphPad Prism9 software. Statistical analysis: One-way ANOVA followed by Tukey's analysis was used for comparison between multiple groups using GraphPad Prism9 software. P values of less than 0.05 (95% confidence interval) are considered significant (ns $p < 0.12$, * p 0.033, ** $p < 0.002$, *** $p < 0.001$).

7. Live/Dead staining

Positive CAIX expression cells (MDA-MB-231) were seeded on a 6-well cell culture plate at 2 x 10^5/well and incubated at 37 ºC for 24 h. After that, the cells were incubated with 0.5 μM of **AZB-I-CAIX$_2$** for 6 h. Then, the cells were washed three times with 0.01 M of PBS buffer (pH 7.4) After incubation, the cells were irradiated by a red LED lamp (660 nm, power density of 8.7 mW cm^{-2}) for 10 min before re-incubation for another 24 h. Thereafter, the cells were stained with 4 μM calcein-AM and propidium iodide (PI) (Thermo Fisher Scientific) for 5 min, and then imaged by Fluorescence microscope (BioRad/Zoe) using λ_{ex} = 490 nm and λ_{em} = 515 nm for calcein AM and λ_{ex} = 535 nm and λ_{em} = 615 nm for PI.

8. Intracellular Singlet Oxygen Generation

Positive CAIX expression cell line (MDA-MB-231) was seeded on 8-well chambered coverglass (LabTek, Nunc) at 1 x 10^4/well and incubated at 37 ºC for 24 h. After that, the cells were incubated with 0.125 and 0.25 μM of **AZB-I-CAIX$_2$** for 6 h. Then, the cells were washed three times with 0.01 M of PBS buffer (pH 7.4). Thereafter, 20 μM of 2,7-dichloro-dihydro-fluorescein diacetate (DCFH-DA, Sigma-Aldrich) was incubated in the cells for 1 h. The cells were washed three times with 0.01 M of PBS buffer (pH 7.4) and irradiated with a red LED lamp (660 nm, power density of 8.7 mW cm^{-2}) for 10 min. Before imaging, the cells were treated with media containing 1.0 μM Hoechst33342 for 10 min. The cells were visualized under 60X oil immersion objective lens by Laser Scanning Confocal Microscope (Nikon A1Rsi) with 561 nm laser (**AZB-I-CAIX$_2$**) and 405 nm laser (Hoechst33342).

9. Murine cell internalization under hypoxia condition

Murine cell lines (4T1 and 67NR) were seeded on 8-well chambered coverglass (LabTek, Nunc) at 1 x 10^4/well and incubated at 37 ºC for 24 h. After that, the cells were incubated under normoxia (humidified 95% air, 5% CO_2 atmosphere) and hypoxia (5% pO_2) conditions for 12 h. Then, the cells were treated with 5 μM of **AZB-I-CAIX$_2$** in DMEM for 0, 1, 3, and 6 h. Thereafter, the cells were washed three times with 0.01 M PBS buffer (pH 7.4) and treated with media containing 1.0 μM Hoechst33342 for 10 min.

Confocal images were visualized under 60 X oil immersion objective lens by Laser Scanning Confocal Microscope (Nikon A1Rsi) with 561 nm laser (**AZB-I-CAIX$_2$**) and 405 nm laser (Hoechst33342).

10. Murine cell cytotoxicity assay under hypoxia condition

4T1 has seeded on a 96-well plate approximately 7×10^3 cells per well and incubated in completed media for 24 h. Thereafter, the cells were incubated under normoxic (humidified 95% air, 5% CO_2 atmosphere) and hypoxic (5% pO_2) conditions at 37 ºC for 12 h before being treated with 0, 0.125. 0.25, 0.5, 5, 10 μM of **AZB-I-CAIX$_2$** for 6 h. After incubation, the cells were washed twice with 0.01 M of PBS buffer (pH 7.4) to remove excess probes and added to the completed media before being irradiated with a red LED lamp (660 nm, power density of 8.7 mW cm^{-2}) for 0, 5, 10, and 15 min and continued culturing for 24 h in dark. Cell viability was detected by 20 μL of methylthiazolyldiphenyl-tetrazolium bromide (MTT reagent, 0.5 mg mL−1, Sigma-Aldrich) for 2.5 h incubation time. After media removal, DMSO was added to dissolve the formazan product and detected through UV-vis absorption of formazan at wavelength 560 nm (BMG Labtech/SPECTROstar Nano microplate reader). IC_{50} values of cell viability were evaluated by GraphPad Prism9 software. Statistical analysis: t-test followed using GraphPad Prism9 software. P values of less than 0.05 (95% confidence interval) are considered significant (ns $p < 0.12$, * $p < 0.033$, ** $p < 0.002$, *** $p < 0.001$).

11. Animal model

Female, 6-8 weeks old wild-type Balb/C mice were purchased from the Animal Experimental Unit, University of Malaya, Malaysia. The mice were maintained in the animal facility at Management and Science University, and all experimental procedures were performed accordingly to the protocol approved by the University Ethics Committee of Management and Science University (Approval code: MSU-RMC-02/FR01/08/L3/001).

12. *In vivo* acute toxicity study

The acute toxicity study on healthy mice (n=2) was assessed through intravenous administration of 30 mg/kg **AZB-I-CAIX$_2$**, 24.60 mg/kg **AZB-I-Control** (Equiv. to 30 mg/kg **AZB-I-CAIX$_2$**), and 12.5 mg/kg acetazolamide (Equiv. to 100 mg/kg **AZB-I-CAIX$_2$**). The toxicity signs were observed based on the Berlin test of typical symptoms including bodyweight loss, ruffled hair, and behavioral changes for 14 days.

13. *In vivo* Photodynamic Therapy

The fur of Balb/C mice was shaved and murine 4T1 breast carcinoma cell lines at a density of 5 x 10^5 cells/mouse were orthotopically injected into the mice's mammary fat pads. **AZB-I-CAIX$_2$**, **AZB-I-Control,** and acetazolamide were dissolved respectively in a cocktail of 2.5% cremophore EL and 2.5% ethanol, and further resuspended in the saline to a volume of 0.2 mL, for injection. The 4T1 breast tumor growth was observed and measured daily until the tumor size reached 150-180 mm^3 (for high CAIX expression).[23] Once the tumor growth reached 150-180 mm^3, the mice were randomly divided into groups for the experiment. The 4T1 tumor-bearing Balb/c mice were treated intravenously with saline, **AZB-I-CAIX$_2$** (30 mg/kg), **AZB-I-Control** (24.60 mg/kg equiv. to 30 mg/kg **AZB-I-CAIX$_2$**), and acetazolamide (3.75 mg/kg equiv. to 30 mg/kg **AZB-I-CAIX$_2$**). The mice were then kept in the dark for 1 hour. After 1-hour administration, the mice were administered with an anesthesia cocktail of 0.1 mL ketamine (90 mg/kg ketamine and 10 mg/kg xylazine) intraperitoneally. The mice were irradiated by using Lumacare LC-122A fiber-optic light delivery system at 80 J for 8 minutes (Fluence rate: 160mW). The tumor size was then observed and measured every 2 days using a digital caliper. Tumor volume was calculated using the formula [(L x W^2)/2], where the reading for L is the longest dimension and W is the shortest dimension.

14. Statistical Analysis for *in vivo*

The result was analyzed using SPSS (IBM version 21). For *in vivo* analysis, one-way ANOVA (Dunnett's test) was used for multi-group comparison. A *p*-value less than 0.05 ($p < 0.05$) indicates statistically significant.

Results and Discussion

*Synthesis of **AZB-I-CAIX$_2$** and **AZB-I-control***

AZB-I-CAIX$_2$ was synthesized via the azide-alkyne Huisgen cycloaddition between two AZ moieties (**2**) and terminal alkynes of an iodo-aza-BODIPY derivative (**4**), prepared by amide coupling between amino aza-BODIPY (AZB-NH$_2$)[19] and 5-hexynoic acids followed by mono-iodination. **AZB-I-control** was produced by a similar reaction condition, except for the linker without AZ (**1**) was used (Scheme 1 and ESI).

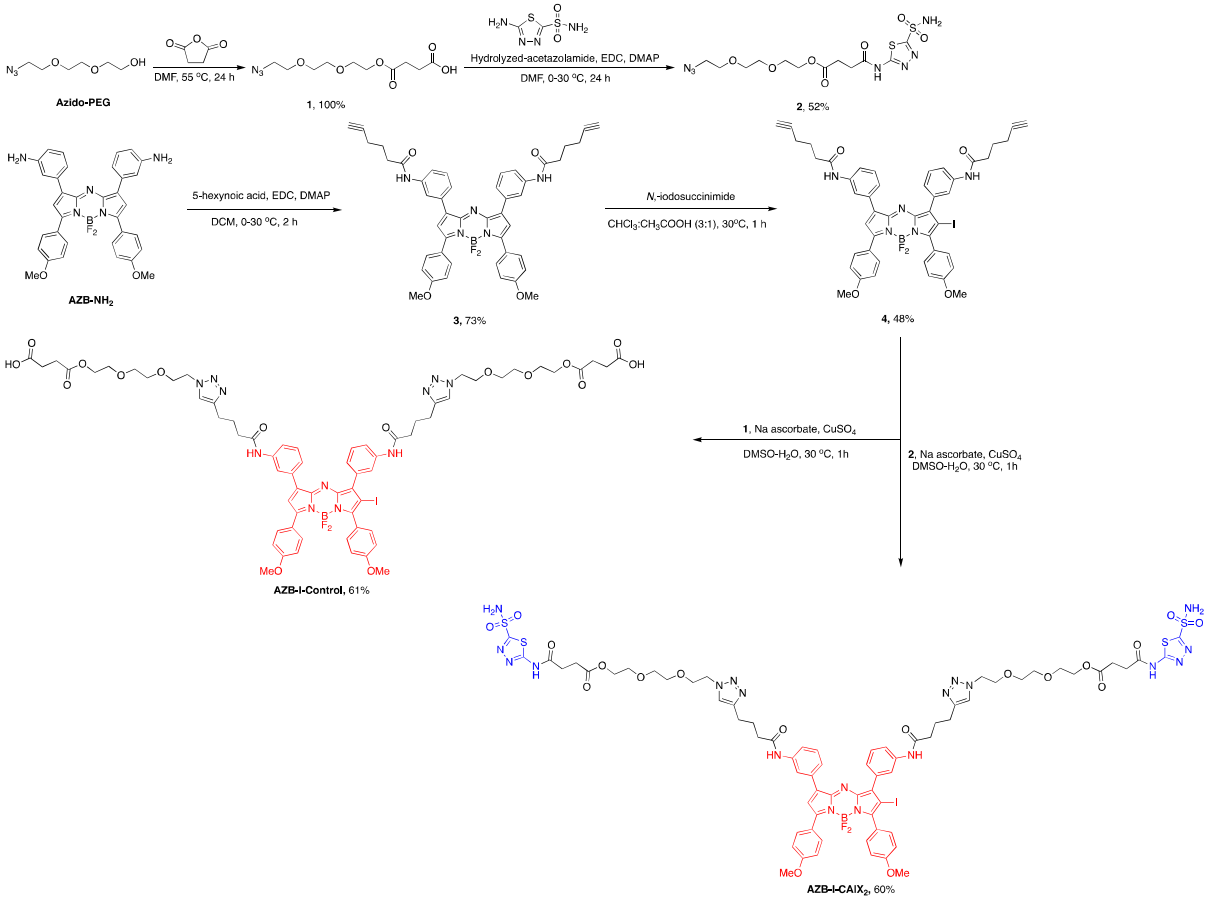

Scheme 1. Synthetic scheme of **AZB-I-CAIX$_2$** and **AZB-I-control**

In general, when heavy atoms are present in the dye structure, *i.e.* aza-BODIPY, the fluorescent emission is usually quenched due to an increase in the rate of triplet formation that affects orbital spin interaction, the so-called heavy atom effect.[24] However, this feature increases singlet oxygen generation which is beneficial for PDT.[20] As a result, aza-BODIPY was mono iodinated in this design to ensure that the fluorescent signal is preserved while the singlet oxygen yield is sufficient for PDT efficiency.

*Photophysical properties of **AZB-I-CAIX$_2$** and **AZB-I-control***

The photophysical properties of **AZB-I-CAIX$_2$** and **AZB-I-control** were investigated by UV-VIS-NIR and fluorescence spectrophotometry in various solvents, as shown in Table 1, Figure 2, and S2. According to the absorbance spectra, **AZB-I-CAIX$_2$** and **AZB-I-control** show similar absorption maxima from 675 to 686 nm in chloroform, DMSO, methanol, and phosphate buffer saline (PBS). The emission maxima are in the range of 713-728 nm in the tested solvents, with fluorescent quantum yield ranging from 0.02-0.09 (Table 1). Similar photophysical properties are observed in the case of **AZB-I-control** (Figure S2 and Table 1).

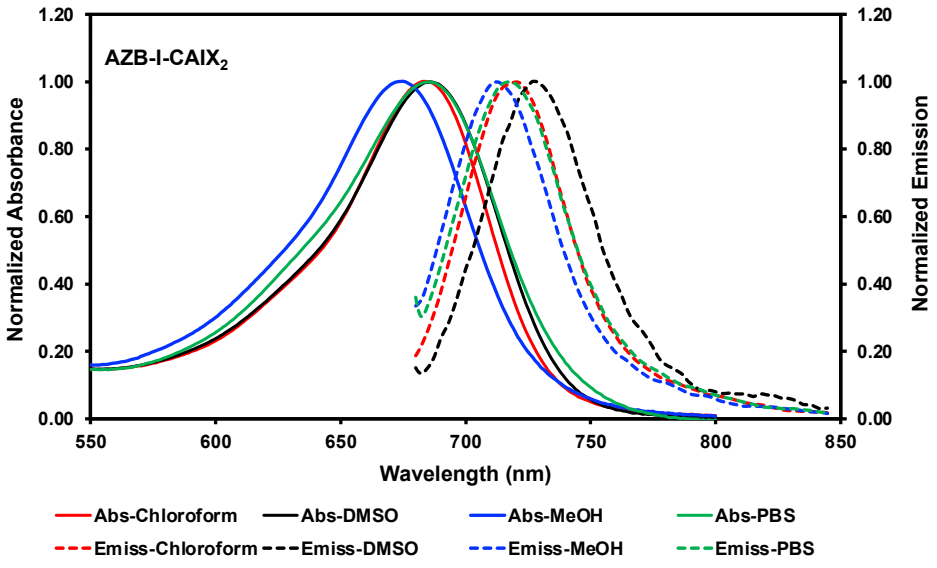

Figure 2. Normalized Vis-NIR absorption and emission spectra of **AZB-I-CAIX$_2$** in various solvents.

Table 1. Photophysical properties of **AZB-I-CAIX$_2$** and **AZB-I-control** (1 μM)

Compound	Solvent	λ_{max} (nm)	ε ($M^{-1} cm^{-1}$)	λ_{emiss} [a] (nm)	Δλ (nm)	Φ_f [b]
AZB-I-CAIX$_2$	$CHCl_3$	683	11.2×10^4	720	37	0.09
	DMSO	686	11.6×10^4	728	42	0.02
	MeOH	675	9.6×10^4	713	38	0.03
	PBS[c]	685	8.9×10^4	718	33	0.05
AZB-I-Control	$CHCl_3$	683	6.0×10^4	720	34	0.14
	DMSO	686	6.5×10^4	728	42	0.04
	MeOH	675	6.6×10^4	714	40	0.05
	PBS[c]	686	6.4×10^4	717	31	0.09

[a] Samples were excited at 670 nm. [b] Relative to Zn-phthalocyanine in pyridine (Φ_f =0.30).

[c] PBS + 3% tween-80.

As the data show that **AZB-I-CAIX$_2$** and **AZB-I-control** have low fluorescent quantum yields according to the heavy atom effect[20], therefore, the singlet oxygen quantum yields of both probes were also investigated. Singlet oxygen generation efficiency of **AZB-I-CAIX$_2$** and **AZB-I-control** was measured using 1,3-diphenylisobenzofuran (DPBF) as singlet oxygen ($^1O_2$) scavenger. After **AZB-I-CAIX$_2$** and **AZB-I-control** were exposed to the light (660 nm, power density 8.7 mW cm^{-2}), $^1O_2$ was produced within a few seconds in an irradiation time-dependent manner, as indicated by the decreasing DPBF absorbance at 408 nm (Figure S3&S4). Moreover, **AZB-I-CAIX$_2$** and **AZB-I-control** could generate $^1O_2$ at a faster rate than methylene blue (standard photosensitizer) in DMSO solution. The calculated singlet oxygen

quantum yields (Φ_Δ) of **AZB-I-CAIX$_2$** and **AZB-I-control** were 0.88 and 0.83, respectively, relative to methylene blue. Therefore, both probes could be good for PDT agents with moderate imaging properties.

Cell internalization and CAIX targeting

To evaluate cancer cell targetability of **AZB-I-CAIX$_2$**, human cancer cell lines with high expression levels of CAIX (MDA-MB-231)[25] and low CAIX levels (MCF-7, HeLa, and A549)[25] were selected for comparison. Moreover, human embryonic kidney cells (HEK-293) were also used as normal cell control.[26] As shown in Figure 3, time-dependent cellular internalization revealed that **AZB-I-CAIX$_2$** faster internalized and accumulated a higher amount in MDA-MB-231 cells from 1 to 24 h incubation time. Whereas low fluorescent signals of **AZB-I-CAIX$_2$** were observed from other cell lines even at the longest exposure time, 24 h (Figure 3A). Quantitative fluorescent signals from all cell lines by ImageJ were presented in Figure 3B. In addition, when **AZB-I-control** was used in the same experiment settings, no observable fluorescent signals were detected from both CAIX positive and negative cells (Figure S5). Furthermore, we performed dose-dependent cell internalization in MDA-MB-231 cells and discovered that 5 μM **AZB-I-CAIX$_2$** provided a clear signal, which will be the best dose for the rest of the in vitro tests (Figure S6). Additionally, when MDA-MB-231 (CAIX+) and MCF-7 (CAIX–) breast cancer lines were co-cultured and then treated with **AZB-I-CAIX$_2$**, the NIR fluorescent signals were only found in the CAIX+ cells (Figure 3C). These findings revealed that **AZB-I-CAIX$_2$** had high selectivity for CAIX when it internalized cancer cells.

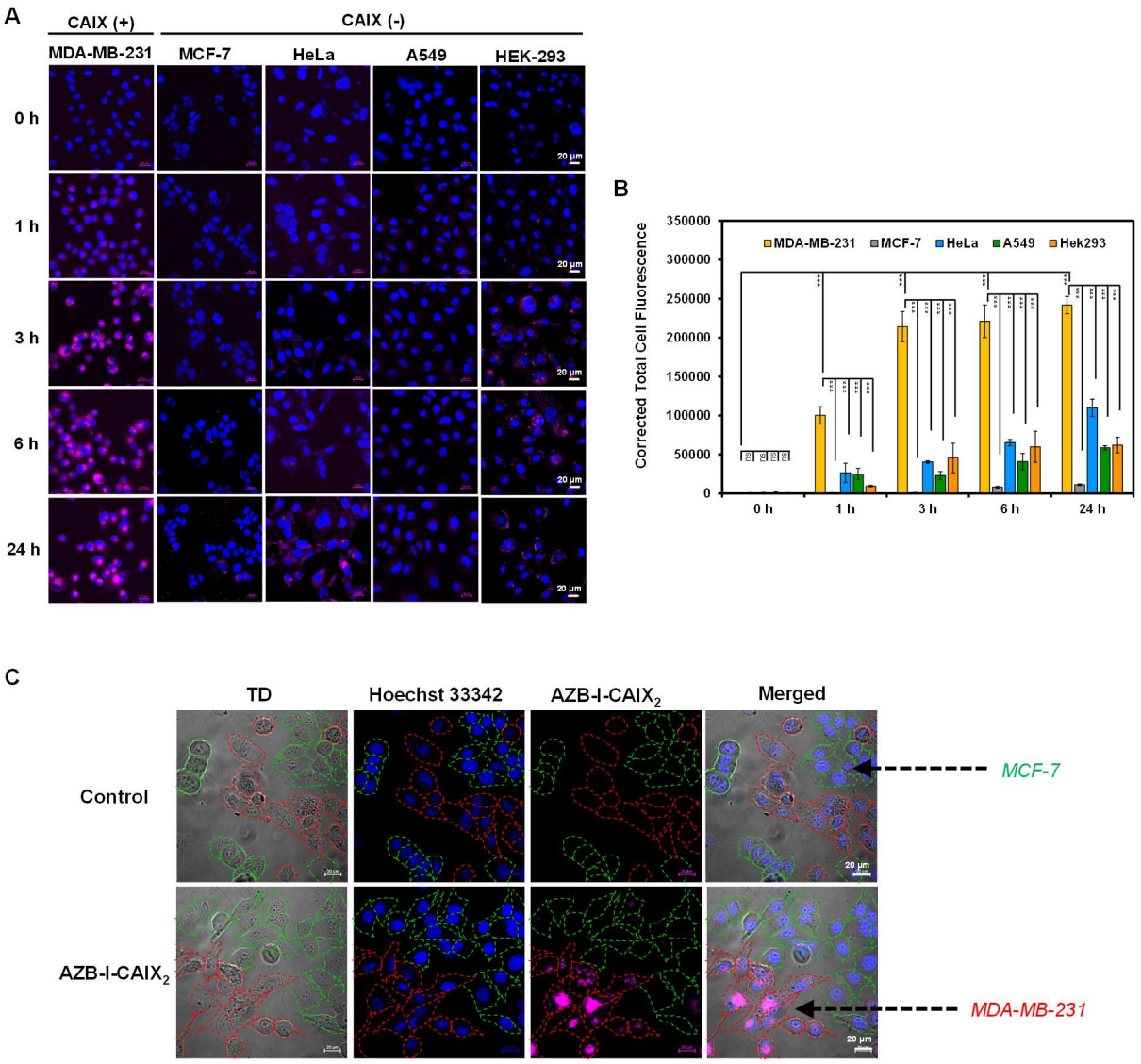

Figure 3. Selective CAIX-dependent uptake of AZB-I-CAIX$_2$ on various cells. (A) Time-dependent cell internalization of **AZB-I-CAIX$_2$** tested on CAIX+ (MDA-MB-231) and CAIX- (MCF-7, HeLa, A549, HEK-293) cells. (B) Corrected Total Cell Fluorescence (CTCF) of signals from experiment A. (C) Confocal images of **AZB-I-CAIX$_2$** internalized CAIX+ (MDA-MB-231) and CAIX- (MCF-7) in the co-culture system. Statistical analysis: One-way ANOVA followed by Tukey's analysis was used for comparison between multiple groups using GraphPad Prism9 software. P values of less than 0.05 (95% confidence interval) are considered significant (ns $p < 0.12$, * $p < 0.033$, ** $p < 0.002$, *** $p < 0.001$). Scale bar = 20 µm.

To further demonstrate the selectivity of **AZB-I-CAIX$_2$**, a competition assay was performed to validate the CAIX-mediated uptake of **AZB-I-CAIX$_2$** in cancer cells. MDA-MB-231 cells were incubated with **AZB-I-CAIX$_2$** (5 μM) in the presence of various concentrations (0, 0.5, and 1.0 mM) of CAIX inhibitor, acetazolamide, for 6 h. The cellular uptake of **AZB-I-CAIX$_2$** was inhibited by CAIX inhibitor in a dose-dependent manner (Figure 4A, 4B and S7). In addition, when a shorter time incubation was used in the competitive assay (1 h and 3 h vs. 6 h), the fluorescent signals were reduced in the presence of acetazolamide at all time points (Figure S8), confirming that acetazolamide moieties play a key role in cellular internalization.

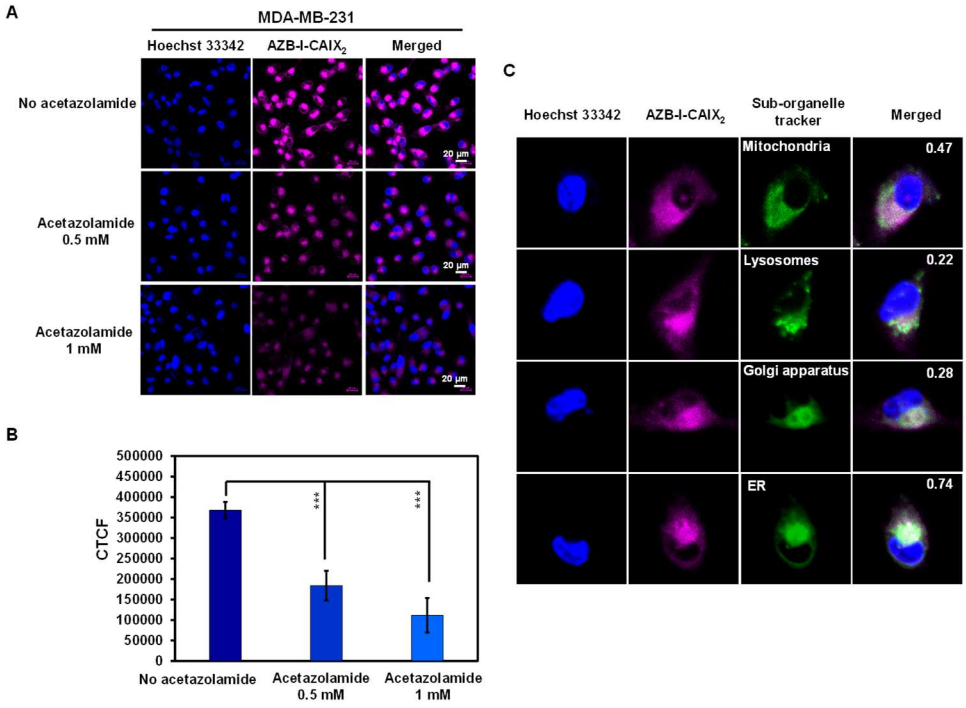

Figure 4. Inhibitory effect of CAIX inhibitor (acetazolamide) on the cellular uptake of **AZB-I-CAIX$_2$**. (A) Confocal images of MDA-MB-231 cells incubated with **AZB-I-CAIX$_2$** (5 μM) in the absence and presence of acetazolamide (0.5 and 1.0 mM) for 6 h. (B) Corrected Total Cell Fluorescence (CTCF) of signals from experiment A. (C) Colocalization of **AZB-I-CAIX$_2$** with organelle trackers (MitoTracker, LysoTracker,

Golgi and ER markers) in MDA-MB-231 cells with Pearson's coefficients of 0.47, 0.22, 0.28 and 0.74, respectively. Scale bar = 20 μm.

In addition to cellular uptake, the detected fluorescent signals of **AZB-I-CAIX$_2$** from MDA-MB-231 cells were found to be colocalized to some degree with MitoTracker, LysoTracker, Golgi, and ER markers with Pearson's coefficients of 0.47, 0.22, 0.28, and 0.74, respectively (Figure 4C). This confirms that our probe can be localized inside the cancer cells and may indicate the internalization of CAIX in response to **AZB-I-CAIX$_2$** binding. [27] CAIX internalization has been studied through caveolar-mediated endocytosis[28] thus suggesting that caveolin-1 protein mediating caveolar-dependent endocytosis might bind to endoplasmic reticulum membrane during endocytic uptake.[29]

In vitro photodynamic therapy

To evaluate the effect of CAIX inhibitor on PDT, assays to measure photocytotoxicity of **AZB-I-CAIX$_2$** in all cell lines including CAIX+, CAIX- and normal cells were performed. All cells were treated with various doses (0-10 μM) of **AZB-I-CAIX$_2$** for 6 h before light irradiation (660 nm, power density of 8.7 mW cm^{-2}) with different durations (0, 5, 10, and 15 min) and then the cells were cultured in the dark for another 24 h. As shown in Figures 5 and S9, **AZB-I-CAIX$_2$** did not cause cytotoxicity to any cells that were not illuminated (0 min). However, once the irradiation was on, the cell viability of all cells was decreasing as the dose of **AZB-I-CAIX$_2$** was increased. Remarkably, MDA-MB-231 (CAIX+) is the most sensitive cell to **AZB-I-CAIX$_2$**. After the cells were irradiated for 5 min, the viability of MDA-MB-231 cells was reduced to 50% at a very low concentration with the half-maximal inhibitory concentration (IC_{50}) of 0.27 μM. In addition, the probe even causes more photocytotoxicity when irradiation time was longer (10 and 15 min) in a dose-dependent manner. On the other hand, after 5 min irradiation, all CAIX–

including normal cells did not show phototoxicity until the concentration of **AZB-I-CAIX$_2$** was up to 5 μM. When CAIX+ cells were irradiated for only 5 min, IC_{50} values of **AZB-I-CAIX$_2$** were more than 15 times lower than those of CAIX- cells (Figure 5). However, prolonged light exposure time did not significantly improve the therapeutic index of **AZB-I-CAIX$_2$** in CAIX+ cells. In contrast, the light dose clearly affected cell viabilities of CAIX- cells.

Furthermore, **AZB-I-control** (no AZ conjugate) was used to test photo-induced cell toxicity on breast cancer lines (MDA-MD-231 and MCF-7) (Figure S9). No dramatic change in cell viability was observed from both cell lines (CAIX+ and CAIX-) even with light irradiation for up to 15 min and compound concentration was up to 10 μM (Figure S10). These findings support the importance of AZ moieties in **AZB-I-CAIX$_2$** for cancer cell uptake through CAIX.

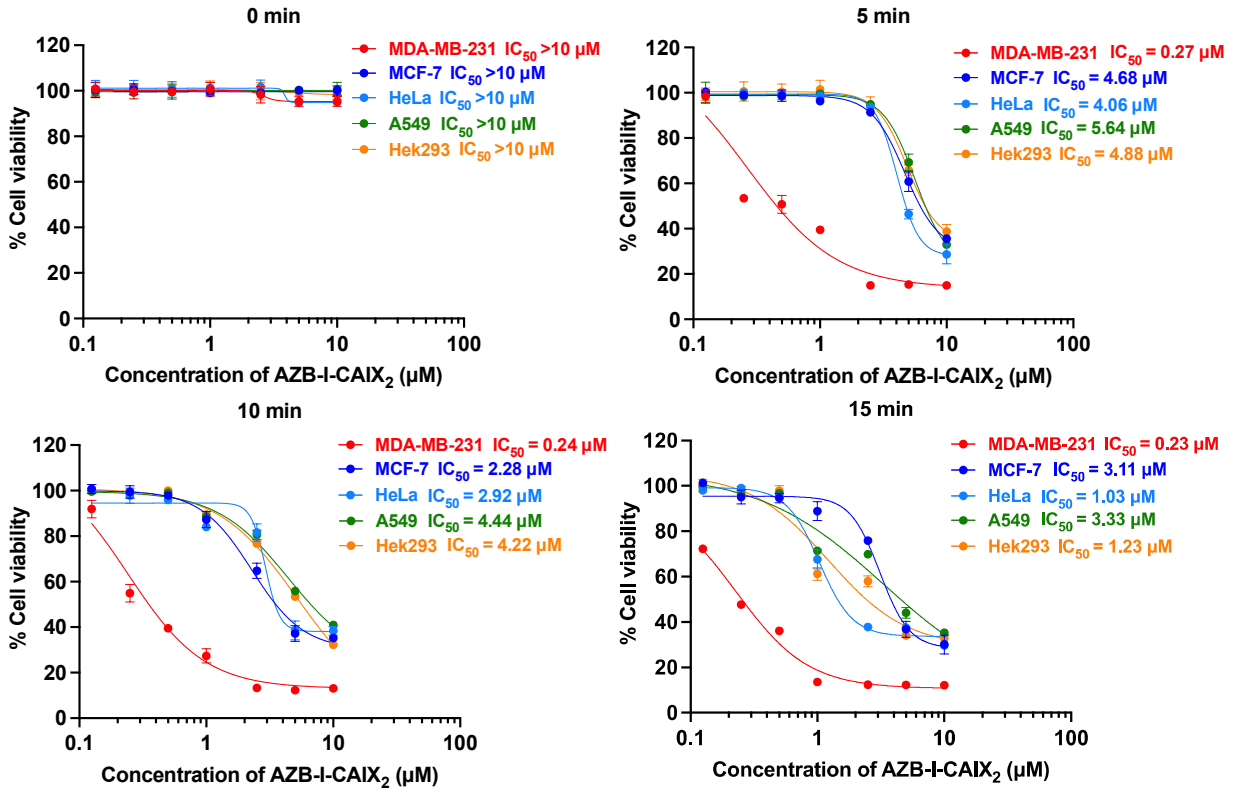

Figure 5. Half maximal inhibitory concentration (IC_{50}) curves of **AZB-I-CAIX$_2$** tested on CAIX+ (MDA-MB-231) and CAIX- (MCF-7, HeLa, A549, HEK-293) cells under various light exposure times (0, 5, 10, 15 min). The cells were incubated with various concentrations of **AZB-I-CAIX$_2$** (0–10 μM) for 6 h and irradiated with a lamp (660 nm, power density of 8.7 mW cm^{-2}). IC_{50} was evaluated using GraphPad Prism9 software.

Live/dead cell staining and intracellular reactive oxygen species detection

To further confirm the CAIX+ cancer cells were destroyed by reactive oxygen species (ROS) from light activation reaction, viability/cytotoxicity and intracellular ROS detection assays were performed. Viable and dead cells were visualized using calcein-AM and propidium iodide (PI) staining. Once calcein-AM enters live cells, green fluorescence can be observed after the dye is cleaved by intracellular esterase, while PI only interacts with dead cells nuclei and gives red fluorescence.

As shown in Figure 6A, after cells were incubated with **AZB-I-CAIX$_2$** followed by light irradiation, a high number of dead cells (indicated as red signal) could be observed from MDA-MB-231 while the live cells (indicated as green signal) were very few. Other CAIX- cancer cells showed some dead cell signals along with a high population of viable cells. Moreover, little to no dead cells were detected in the case of the normal cell (HEK-293). In addition, all the cells incubated with **AZB-I-CAIX$_2$** (no light irradiation) and cells incubated with **AZB-I-control** (either with or without illumination) mostly remained viable (Figure S11).

Subsequent, 2′,7′-dichlorofluorescein diacetate (DCFH-DA) was utilized to monitor intracellular ROS generation because its non-fluorescent form can be oxidized by ROS to create the fluorescence 2′,7′-dichlorofluorescein (DCF) that exhibits green fluorescence inside living cells. As shown in Figure 6B, bright green emission is observed only in the case of MDA-MB-231 cells incubated with **AZB-I-CAIX$_2$**

followed by light activation. The green fluorescence increases when a higher amount of **AZB-I-CAIX$_2$** was used, implying the ROS was generated from our probe inside the cells in the dose-response relationship.

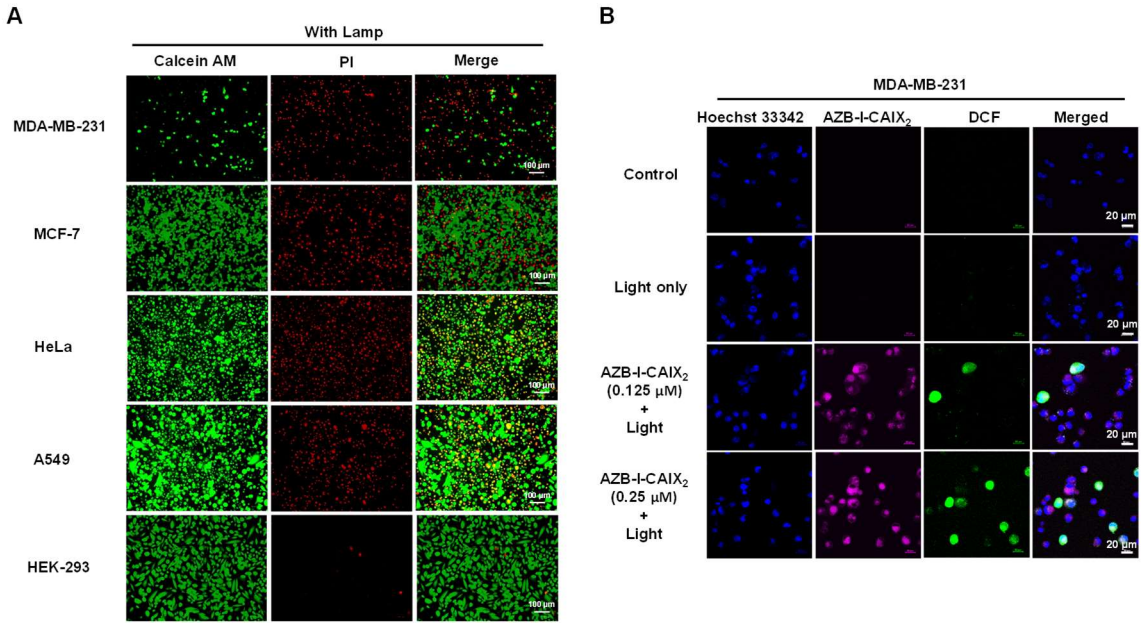

Figure 6. Viability/Cytotoxicity assay and intracellular ROS detection. (A) Live/dead cell imaging of CAIX+ (MDA-MB-231) and CAIX- (MCF-7, HeLa, A549, HEK-293) cells incubated with **AZB-I-CAIX$_2$** (0.5 μM) under 10 min light irradiation. (B) Confocal images of MDA-MB-231 cells incubated with **AZB-I-CAIX$_2$** (0.125 and 0.5 μM) and light irradiation for 10 min in the presence of ROS detection probe, DCFH-DA. The green emission signal indicated the existence of ROS inside the cells.

Murine cells study in hypoxia condition

Two murine breast cancer lines were used as a comparison. 4T1 cells are highly metastatic breast cancer cells. When compared to nonmetastatic 67NR cells, tumors that formed by 4T1 have significantly higher amounts of hypoxia, necrosis, and apoptosis due to fewer blood vessels. In addition, the bioinformatic analysis revealed several hypoxia-regulated genes, including CAIX, that are expressed at

higher levels in the 4T1 tumors relative to the 67NR. Therefore, the 4T1 mouse could be a suitable model to study the effect of overexpression of CAIX on the progression of breast cancer.[30]

4T1 and 67NR cells internalization experiments were performed under normoxia and hypoxia conditions. **AZB-I-CAIX$_2$** could be observed only from hypoxic 4T1 cells after 1 h incubation (Figure 7A) and the fluorescence increased in a time-dependent manner. After 6 hours of treatment with **AZB-I-CAIX$_2$**, 4T1 cells (normoxic and hypoxic) were exposed to light (660 nm) for various time periods (0, 5, 10, and 15 min). As shown in IC_{50} curves (Figure 7B), hypoxic cells were more sensitive to light compared to normoxic ones and the IC_{50} of hypoxic 4T1 cells was lower with longer exposure duration. These results suggest that under hypoxia, 4T1 expresses higher levels of CAIX, allowing **AZB-I-CAIX$_2$** to be internalized more efficiently, resulting in a greater accumulation of tumor cells. Importantly, PDT remained active even in the presence of low oxygen concentrations, indicating that the inclusion of a CAIX inhibitor can boost PDT's therapeutic impact.

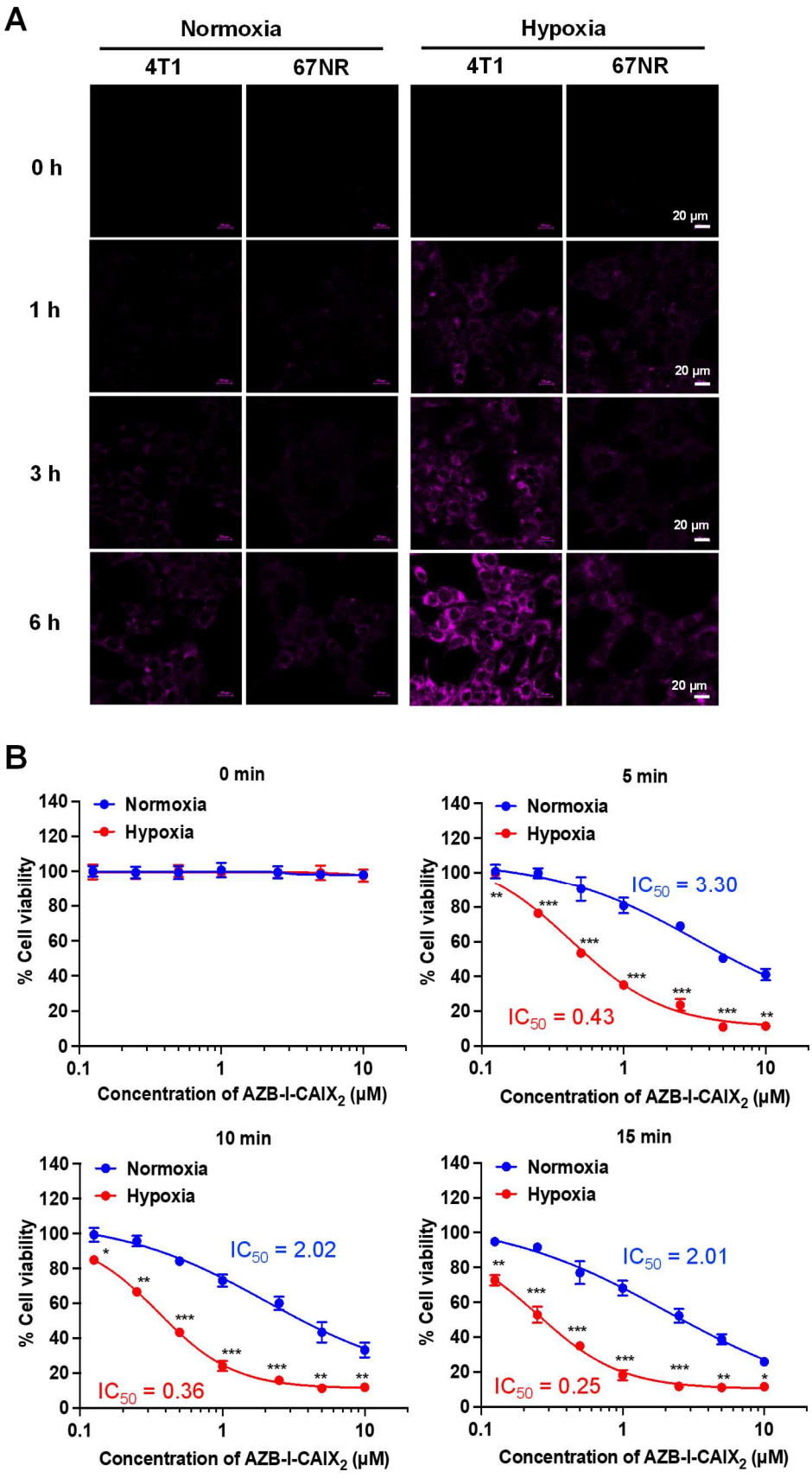
A
Normoxia
Hypoxia
4T1
67NR
4T1
67NR
0 h
1 h
3 h
6 h
20 μm
B
0 min
5 min
10 min
15 min
Normoxia
Hypoxia
% Cell viability
Concentration of AZB-I-CAIX2 (μM)
IC50 = 3.30
IC50 = 0.43
IC50 = 2.02
IC50 = 0.36
IC50 = 2.01
IC50 = 0.25

Figure 7. (A) Time-dependent cell internalization of **AZB-I-CAIX$_2$** under normoxia and hypoxia conditions of 4T1 and 67NR cells. (B) IC_{50} curves of 4T1 cells incubated with **AZB-I-CAIX$_2$** for 6 h before light illumination for 0, 5, 10, and 15 min.

*In vivo a*cute toxicity study

The conjugates were then tested for acute toxicity in Balb/c mice. Intravenous administration of 30 mg/kg **AZB-I-CAIX$_2$**, 24.60 mg/kg **AZB-I-Control** (equiv. to 30mg/kg **AZB-I-CAIX$_2$**), and 12.5 mg/kg acetazolamide (equiv. to 100 mg/kg **AZB-I-CAIX$_2$**) showed no sign of toxicity such as apathy, weight loss, ruffled hair or behavioral changes up to 14 days of observation. No sudden weight loss was recorded, with constant weight (gram) post-administration (Figure 8A). Hence, 30 mg/kg of **AZB-I-CAIX$_2$** was chosen for the antitumor study.

In vivo photodynamic therapy

Antitumor efficacy of **AZB-I-CAIX$_2$**, **AZB-I-Control,** and acetazolamide was compared in 4T1 tumor-bearing mice following PDT. In the absence of the photosensitizer, irradiation of the tumor tissue with light at an optimum light dose will not induce tumor necrosis. As shown in Figure 8B, tumor necrosis (black area) only appeared in the mice treated with **AZB-I-CAIX$_2$** at 30 mg/kg, starting at day-3 post-PDT. However, saline, **AZB-I-Control**, and acetazolamide control group-treated mice show progressive tumor growth, with no necrotic tumor tissue found from day-3 until day-7 post-PDT. Although the **AZB-I-Control** was used, tumor destruction was not observed, probably due to the poor accumulation in the tumor tissue. Hence, suggests the selective accumulation of **AZB-I-CAIX$_2$** in the 4T1 tumor tissue at 1 h post intravenous administration to mediate PDT-induced necrotic tissue. In comparing the tumor volume in every group as shown in Figure 8C, **AZB-I-CAIX$_2$** significantly reduced the tumor volume by 76.4% on day-3 compared to pre-PDT and remained smaller size throughout 21 days of observation ($p < 0.0001$). In contrast, administration of 24.60 mg/kg **AZB-I-Control** (Equiv. to 30 mg/kg **AZB-I-CAIX$_2$**) and 3.75

mg/kg acetazolamide (Equiv. to 30 mg/kg **AZB-I-CAIX$_2$**) treated groups showed no tumor shrinkage at day-3 post-PDT. An analysis in comparing entire tumor volume over time was performed between groups. As shown in Figure 8D, the **AZB-I-CAIX$_2$** treatment group has 85.7% lower tumor volume ($p < 0.0001$), followed by 55.9% in acetazolamide ($p < 0.001$) and 24.4% in **AZB-I-Control** ($p = 0.232$) compared to the control group. This suggested that the **CAIX$_2$** ligand has improved the delivery of **AZB-I** to CAIX+ tumor. Administration of acetazolamide showed 55.9% lower tumor volume compared to the control group, this is parallel with other studies as reported CAIX-Inhibitor acetazolamide able to reduce the tumor growth, invasiveness, and proliferation of cancer cells.[31]

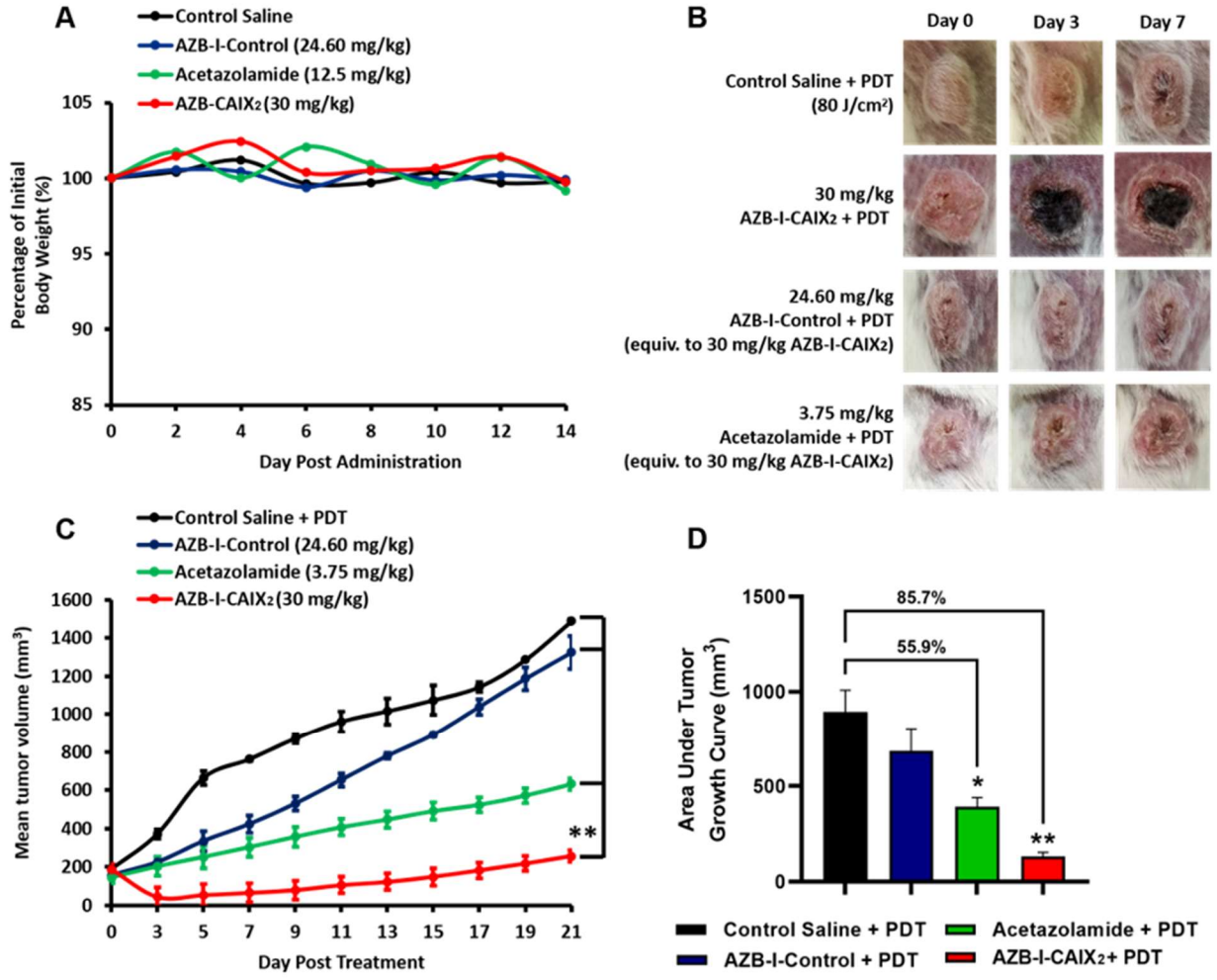

Figure 8. *In vivo* acute toxicity and antitumor efficacy of **AZB-I-CAIX$_2$**, **AZB-I-Control,** and acetazolamide without irradiation. (A) Percentage of mice body weight (n = 2) for *in vivo* acute toxicity study throughout 14 days of observation. (B) Gross observation of tumor at days 0, 3, and 7 post-PDT. The figure in each group is representative of n = 6 mice. (C) 4T1 tumor volume **post-AZB-I-CAIX$_2$**, **AZB-I-Control** and acetazolamide treatment, and PDT. ** $p < 0.0001$ for **AZB-I-CAIX$_2$** *vs* control saline, **AZB-I-Control,** and acetazolamide at all time points. (D) The area under the tumor volume in **AZB-I-CAIX$_2$, AZB-I-Control,** and acetazolamide throughout 21 days of analysis. The graph represents mean ± SEM (n = 6), * $p < 0.001$ and ** $p < 0.0001$ compared to control saline, using One Way ANOVA (Dunnett's).

Conclusions

The combination of CAIX inhibition and NIR photosensitizer has tremendous potential for overcoming hypoxic restrictions in PDT. We designed a CAIX-targeting NIR photosensitizer (**AZB-I-CAIX$_2$**) that contains two acetazolamide and aza-BODIPY moieties to offer a singlet oxygen-producing photosensitizer while permitting fluorescence-based cell internalization tracking. **AZB-I-control** was offered as a control, a comparable aza-BODIPY structure without acetazolamide units, that just has a PDT impact and no ability to target. *In vitro* studies revealed that **AZB-I-CAIX$_2$** was preferentially localized to the ER and selectively internalized in human breast cancer cells that overexpress CAIX (CAIX+, MDA-MB-231), whereas **AZB-I-control** did not show any cell uptake. The selectivity of **AZB-I-CAIX$_2$** to CAIX was also confirmed by inhibitory effect and co-cultured of CAIX+ and CAIX- cells. **AZB-I-CAIX$_2$** also produced singlet oxygen quickly after being exposed to 660 nm light and showed selective photo-induced cell cytotoxicity at low doses. Furthermore, under hypoxia-induced CAIX expression in 4T1 cells, **AZB-I-CAIX$_2$** revealed a robust fluorescence response and demonstrated efficient cancer cell ablation by PDT. Finally, in vivo experiments in mice revealed that **AZB-I-CAIX$_2$** had no acute toxicity when used without irradiation, while dramatically lowering tumor mass following light exposure when compared to mice

treated with **AZB-I-control** and acetazolamide. As a result, **AZB-I-CAIX$_2$** could be a useful targeting agent for CAIX-expressing cells, with increased therapeutic efficacy in alleviating PDT-induced hypoxia due to CAIX suppression.

ASSOCIATED CONTENT

Supporting Information.

Compounds characterizations, photophysical properties of the control, singlet oxygen quantum yields, and biological assays are available in the Supporting Information.

AUTHOR INFORMATION

Corresponding Author

Anyanee Kamkaew – School of Chemistry, Institute of Science, Suranaree University of Technology, Nakhon Ratchasima 30000, Thailand. Email: anyanee@sut.ac.th (for compound syntheses and in vitro study)

Chin Siang Kue – Faculty of Health and Life Sciences, Management and Science University, Seksyen 13, 40100 Shah Alam, Selangor, Malaysia. Email: cskue@msu.edu.my (for in vivo study)

Author Contributions

T.P. synthesize the compounds and conceived all the cell experiments. K.C. conducted the photophysical properties and analyzed all spectroscopic data. S.N.B. and C.S.K. conducted in vivo experiments. K.C., R-Y.L., C.S.K., and A.K. validated the results. The manuscript was written through the contributions of all authors. All authors have approved the final version of the manuscript.

Funding Sources

This work was supported by Suranaree University of Technology (SUT), Thailand Science Research and Innovation (TSRI), National Research Council of Thailand (NRCT) under grant number N41A640150, andManagement and Science University Seed Research Grant (SG-003-012020-FHLS).

ACKNOWLEDGMENT

T.P. thanks Suranaree University of Technology (SUT) and the National Research Council of Thailand (NRCT) for her thesis grant. We also thank Dr. Utumporn Ngivprom for HPLC analysis.

REFERENCES

(1) Jung, H. S.; Han, J.; Shi, H.; Koo, S.; Singh, H.; Kim, H.-J.; Sessler, J. L.; Lee, J. Y.; Kim, J.-H.; Kim, J. S. Overcoming the Limits of Hypoxia in Photodynamic Therapy: A Carbonic Anhydrase IX-Targeted Approach. *Journal of the American Chemical Society* **2017**, *139* (22), 7595-7602. DOI: 10.1021/jacs.7b02396.

(2) Lucky, S. S.; Soo, K. C.; Zhang, Y. Nanoparticles in Photodynamic Therapy. *Chemical Reviews* **2015**, *115* (4), 1990-2042. DOI: 10.1021/cr5004198.

(3) Dougherty, T. J.; Gomer, C. J.; Henderson, B. W.; Jori, G.; Kessel, D.; Korbelik, M.; Moan, J.; Peng, Q. Photodynamic therapy. *J Natl Cancer Inst* **1998**, *90* (12), 889-905. DOI: 10.1093/jnci/90.12.889. DeRosa, M. C.; Crutchley, R. J. Photosensitized singlet oxygen and its applications. *Coordin Chem Rev* **2002**, *233*, 351-371. DOI: Pii S0010-8545(02)00034-6

Doi 10.1016/S0010-8545(02)00034-6. Henderson, B. W.; Dougherty, T. J. How does photodynamic therapy work? *Photochem Photobiol* **1992**, *55* (1), 145-157. DOI: 10.1111/j.1751-1097.1992.tb04222.x From NLM.

(4) Dolmans, D. E.; Fukumura, D.; Jain, R. K. Photodynamic therapy for cancer. *Nat Rev Cancer* **2003**, *3* (5), 380-387. DOI: 10.1038/nrc1071.

(5) Hong, E. J.; Choi, D. G.; Shim, M. S. Targeted and effective photodynamic therapy for cancer using functionalized nanomaterials. *Acta Pharmaceutica Sinica B* **2016**, *6* (4), 297-307. DOI: https://doi.org/10.1016/j.apsb.2016.01.007.

(6) Krzykawska-Serda, M.; Dabrowski, J. M.; Arnaut, L. G.; Szczygiel, M.; Urbanska, K.; Stochel, G.; Elas, M. The role of strong hypoxia in tumors after treatment in the outcome of bacteriochlorin-based photodynamic therapy. *Free Radic Biol Med* **2014**, *73*, 239-251. DOI: 10.1016/j.freeradbiomed.2014.05.003. Song, X.; Feng, L.; Liang, C.; Yang, K.; Liu, Z. Ultrasound Triggered Tumor Oxygenation with Oxygen-Shuttle Nanoperfluorocarbon to Overcome Hypoxia-Associated Resistance in Cancer Therapies. *Nano Lett* **2016**, *16* (10), 6145-6153. DOI: 10.1021/acs.nanolett.6b02365. Ding, H.; Yu, H.; Dong, Y.; Tian, R.; Huang, G.; Boothman, D. A.; Sumer, B. D.; Gao, J. Photoactivation switch from type II to type I reactions by electron-rich micelles for improved photodynamic therapy of cancer cells under hypoxia. *Journal of controlled release : official journal of the Controlled Release Society* **2011**, *156* (3), 276-280. DOI: 10.1016/j.jconrel.2011.08.019 PubMed.

(7) Freitas, I.; Baronzio, G. F. Tumor hypoxia, reoxygenation and oxygenation strategies: possible role in photodynamic therapy. *J Photochem Photobiol B* **1991**, *11* (1), 3-30. Koukourakis, M. I.; Giatromanolaki, A.; Skarlatos, J.; Corti, L.; Blandamura, S.; Piazza, M.; Gatter, K. C.; Harris, A. L. Hypoxia inducible factor (HIF-1a and HIF-2a) expression in early esophageal cancer and response to photodynamic therapy and radiotherapy. *Cancer Res* **2001**, *61* (5), 1830-1832. Huang, Z. A review of progress in clinical photodynamic therapy. *Technology in cancer research & treatment* **2005**, *4* (3), 283-293. DOI: 10.1177/153303460500400308 PubMed.

(8) Supuran, C. T. Carbonic anhydrases: novel therapeutic applications for inhibitors and activators. *Nat Rev Drug Discov* **2008**, *7* (2), 168-181. DOI: 10.1038/nrd2467 From NLM. Mahalingam, S. M.; Chu, H.; Liu, X.; Leamon, C. P.; Low, P. S. Carbonic Anhydrase IX-Targeted Near-Infrared Dye for Fluorescence Imaging of Hypoxic Tumors. *Bioconjug Chem* **2018**, *29* (10), 3320-3331. DOI: 10.1021/acs.bioconjchem.8b00509 From NLM.

(9) Supuran, C. T.; Winum, J.-Y. Carbonic anhydrase IX inhibitors in cancer therapy: an update. *Future Medicinal Chemistry* **2015**, *7* (11), 1407-1414. DOI: 10.4155/fmc.15.71 (acccessed 2020/04/10).

(10) Benej, M.; Pastorekova, S.; Pastorek, J. Carbonic anhydrase IX: regulation and role in cancer. *Subcell Biochem* **2014**, *75*, 199-219. DOI: 10.1007/978-94-007-7359-2_11.

(11) McDonald, P. C.; Dedhar, S. Carbonic anhydrase IX (CAIX) as a mediator of hypoxia-induced stress response in cancer cells. *Subcell Biochem* **2014**, *75*, 255-269. DOI: 10.1007/978-94-007-7359-2_13.

(12) Helmlinger, G.; Sckell, A.; Dellian, M.; Forbes, N. S.; Jain, R. K. Acid production in glycolysis-impaired tumors provides new insights into tumor metabolism. *Clin Cancer Res* **2002**, *8* (4), 1284-1291.

(13) Thiry, A.; Dogne, J. M.; Masereel, B.; Supuran, C. T. Targeting tumor-associated carbonic anhydrase IX in cancer therapy. *Trends Pharmacol Sci* **2006**, *27* (11), 566-573. DOI: 10.1016/j.tips.2006.09.002.

(14) Supuran, C. T. Carbonic anhydrase inhibitors. *Bioorg Med Chem Lett* **2010**, *20* (12), 3467-3474. DOI: 10.1016/j.bmcl.2010.05.009. De Simone, G.; Vitale, R. M.; Di Fiore, A.; Pedone, C.; Scozzafava, A.; Montero, J. L.; Winum, J. Y.; Supuran, C. T. Carbonic anhydrase inhibitors: Hypoxia-activatable sulfonamides incorporating disulfide bonds that target the tumor-associated isoform IX. *J Med Chem* **2006**, *49* (18), 5544-5551. DOI: 10.1021/jm060531j. Supuran, C. T.; Winum, J. Y. Carbonic anhydrase IX inhibitors in cancer therapy: an update. *Future Med Chem* **2015**, *7* (11), 1407-1414. DOI: 10.4155/fmc.15.71. Winum, J. Y.; Rami, M.; Scozzafava, A.; Montero, J. L.; Supuran, C. Carbonic anhydrase IX: a new druggable target for the design of antitumor agents. *Med Res Rev* **2008**, *28* (3), 445-

463. DOI: 10.1002/med.20112. Wichert, M.; Krall, N. Targeting carbonic anhydrase IX with small organic ligands. *Curr Opin Chem Biol* **2015**, *26*, 48-54. DOI: 10.1016/j.cbpa.2015.02.005.

(15) Krock, B. L.; Skuli, N.; Simon, M. C. Hypoxia-Induced Angiogenesis: Good and Evil. *Genes & Cancer* **2011**, *2* (12), 1117-1133. DOI: 10.1177/1947601911423654 (acccessed 2022/06/04).

(16) Zhou, R.; Zeng, X.; Zhao, H.; Chen, Q.; Wu, P. Combating the hypoxia limit of photodynamic therapy through reversing the survival-related pathways of cancer cells. *Coordination Chemistry Reviews* **2022**, *452*, 214306. DOI: https://doi.org/10.1016/j.ccr.2021.214306. Zhao, X.; Liu, J.; Fan, J.; Chao, H.; Peng, X. Recent progress in photosensitizers for overcoming the challenges of photodynamic therapy: from molecular design to application. *Chemical Society Reviews* **2021**, *50* (6), 4185-4219, 10.1039/D0CS00173B. DOI: 10.1039/D0CS00173B. Wan, Y.; Fu, L.-H.; Li, C.; Lin, J.; Huang, P. Conquering the Hypoxia Limitation for Photodynamic Therapy. *Advanced Materials* **2021**, *33* (48), 2103978. DOI: https://doi.org/10.1002/adma.202103978. Liang, P.; Ballou, B.; Lv, X.; Si, W.; Bruchez, M. P.; Huang, W.; Dong, X. Monotherapy and Combination Therapy Using Anti-Angiogenic Nanoagents to Fight Cancer. *Advanced Materials* **2021**, *33* (15), 2005155. DOI: https://doi.org/10.1002/adma.202005155. Pucelik, B.; Sulek, A.; Barzowska, A.; Dabrowski, J. M. Recent advances in strategies for overcoming hypoxia in photodynamic therapy of cancer. *Cancer Lett* **2020**, *492*, 116-135. DOI: 10.1016/j.canlet.2020.07.007.

(17) Grosjean, P.; Wagnieres, G.; Fontolliet, C.; van den Bergh, H.; Monnier, P. Clinical photodynamic therapy for superficial cancer in the oesophagus and the bronchi: 514 nm compared with 630 nm light irradiation after sensitization with Photofrin II. *Br J Cancer* **1998**, *77* (11), 1989-1995.

(18) Kamkaew, A.; Burgess, K. Double-targeting using a TrkC ligand conjugated to dipyrrometheneboron difluoride (BODIPY) based photodynamic therapy (PDT) agent. *J Med Chem* **2013**, *56* (19), 7608-7614. DOI: 10.1021/jm4012142. Kue, C. S.; Kamkaew, A.; Lee, H. B.; Chung, L. Y.; Kiew, L. V.; Burgess, K. Targeted PDT agent eradicates TrkC expressing tumors via photodynamic therapy (PDT). *Mol Pharm* **2015**, *12* (1), 212-222. DOI: 10.1021/mp5005564.

(19) Kamkaew, A.; Burgess, K. Aza-BODIPY dyes with enhanced hydrophilicity. *Chem Commun (Camb)* **2015**, *51* (53), 10664-10667. DOI: 10.1039/c5cc03649f.

(20) Kamkaew, A.; Lim, S. H.; Lee, H. B.; Kiew, L. V.; Chung, L. Y.; Burgess, K. BODIPY dyes in photodynamic therapy. *Chem Soc Rev* **2013**, *42* (1), 77-88. DOI: 10.1039/c2cs35216h.

(21) Krall, N.; Pretto, F.; Neri, D. A bivalent small molecule-drug conjugate directed against carbonic anhydrase IX can elicit complete tumour regression in mice. *Chemical Science* **2014**, *5* (9), 3640-3644, 10.1039/C4SC00685B. DOI: 10.1039/C4SC00685B.

(22) Turkmen, H.; Durgun, M.; Yilmaztekin, S.; Emul, M.; Innocenti, A.; Vullo, D.; Scozzafava, A.; Supuran, C. T. Carbonic anhydrase inhibitors. Novel sulfanilamide/acetazolamide derivatives obtained by the tail approach and their interaction with the cytosolic isozymes I and II, and the tumor-associated isozyme IX. *Bioorganic & Medicinal Chemistry Letters* **2005**, *15* (2), 367-372. DOI: https://doi.org/10.1016/j.bmcl.2004.10.070. Waghorn, P. A.; Jones, M. W.; McIntyre, A.; Innocenti, A.; Vullo, D.; Harris, A. L.; Supuran, C. T.; Dilworth, J. R. Targeting Carbonic Anhydrases with Fluorescent BODIPY-Labelled Sulfonamides. *European Journal of Inorganic Chemistry* **2012**, *2012*, 2898-2907. Teruya, K.; Tonissen, K. F.; Poulsen, S.-A. Recent developments of small molecule chemical probes for

fluorescence-based detection of human carbonic anhydrase II and IX. *MedChemComm* **2016**, *7* (11), 2045-2062, 10.1039/C6MD00296J. DOI: 10.1039/C6MD00296J.

(23) Rabbani, Z. N.; Spasojevic, I.; Zhang, X.; Moeller, B. J.; Haberle, S.; Vasquez-Vivar, J.; Dewhirst, M. W.; Vujaskovic, Z.; Batinic-Haberle, I. Antiangiogenic action of redox-modulating Mn(III) meso-tetrakis(N-ethylpyridinium-2-yl)porphyrin, MnTE-2-PyP(5+), via suppression of oxidative stress in a mouse model of breast tumor. *Free Radic Biol Med* **2009**, *47* (7), 992-1004. DOI: 10.1016/j.freeradbiomed.2009.07.001 From NLM.

(24) De Simone, B. C.; Mazzone, G.; Pirillo, J.; Russo, N.; Sicilia, E. Halogen atom effect on the photophysical properties of substituted aza-BODIPY derivatives. *Physical Chemistry Chemical Physics* **2017**, *19* (3), 2530-2536, 10.1039/C6CP07874E. DOI: 10.1039/C6CP07874E.

(25) Jung, H. S.; Han, J.; Shi, H.; Koo, S.; Singh, H.; Kim, H. J.; Sessler, J. L.; Lee, J. Y.; Kim, J. H.; Kim, J. S. Overcoming the Limits of Hypoxia in Photodynamic Therapy: A Carbonic Anhydrase IX-Targeted Approach. *J Am Chem Soc* **2017**, *139* (22), 7595-7602. DOI: 10.1021/jacs.7b02396.

(26) Rana, S.; Nissen, F.; Lindner, T.; Altmann, A.; Mier, W.; Debus, J.; Haberkorn, U.; Askoxylakis, V. Screening of a Novel Peptide Targeting the Proteoglycan-Like Region of Human Carbonic Anhydrase IX. *Molecular Imaging* **2013**, *12* (8), 7290.2013.00066. DOI: 10.2310/7290.2013.00066 (acccessed 2022/06/04).

(27) Hulikova, A.; Zatovicova, M.; Svastova, E.; Ditte, P.; Brasseur, R.; Kettmann, R.; Supuran, C. T.; Kopacek, J.; Pastorek, J.; Pastorekova, S. Intact intracellular tail is critical for proper functioning of the tumor-associated, hypoxia-regulated carbonic anhydrase IX. *FEBS Letters* **2009**, *583* (22), 3563-3568. DOI: https://doi.org/10.1016/j.febslet.2009.10.060.

(28) Bourseau-Guilmain, E.; Menard, J. A.; Lindqvist, E.; Indira Chandran, V.; Christianson, H. C.; Cerezo Magaña, M.; Lidfeldt, J.; Marko-Varga, G.; Welinder, C.; Belting, M. Hypoxia regulates global membrane protein endocytosis through caveolin-1 in cancer cells. *Nature Communications* **2016**, *7* (1), 11371. DOI: 10.1038/ncomms11371.

(29) Schlegel, A.; Arvan, P.; Lisanti, M. P. Caveolin-1 Binding to Endoplasmic Reticulum Membranes and Entry into the Regulated Secretory Pathway Are Regulated by Serine Phosphorylation: PROTEIN SORTING AT THE LEVEL OF THE ENDOPLASMIC RETICULUM *. *Journal of Biological Chemistry* **2001**, *276* (6), 4398-4408. DOI: 10.1074/jbc.M005448200 (acccessed 2022/06/04).

(30) Chafe, S. C.; Lou, Y.; Sceneay, J.; Vallejo, M.; Hamilton, M. J.; McDonald, P. C.; Bennewith, K. L.; Möller, A.; Dedhar, S. Carbonic Anhydrase IX Promotes Myeloid-Derived Suppressor Cell Mobilization and Establishment of a Metastatic Niche by Stimulating G-CSF Production. *Cancer Research* **2015**, *75* (6), 996-1008. DOI: 10.1158/0008-5472.Can-14-3000. Lou, Y.; McDonald, P. C.; Oloumi, A.; Chia, S.; Ostlund, C.; Ahmadi, A.; Kyle, A.; auf dem Keller, U.; Leung, S.; Huntsman, D.; et al. Targeting Tumor Hypoxia: Suppression of Breast Tumor Growth and Metastasis by Novel Carbonic Anhydrase IX Inhibitors. *Cancer Research* **2011**, *71* (9), 3364-3376. DOI: 10.1158/0008-5472.Can-10-4261.

(31) Li, X.-J.; Xiang, Y.; Ma, B.; Qi, X.-Q. Effects of Acetazolamide Combined with or without NaHCO3 on Suppressing Neoplasm Growth, Metastasis and Aquaporin-1 (AQP1) Protein Expression. *International Journal of Molecular Sciences* **2007**, *8* (3). DOI: 10.3390/i8030229. Cianchi, F.; Vinci, M. C.; Supuran, C. T.;

Peruzzi, B.; De Giuli, P.; Fasolis, G.; Perigli, G.; Pastorekova, S.; Papucci, L.; Pini, A.; et al. Selective Inhibition of Carbonic Anhydrase IX Decreases Cell Proliferation and Induces Ceramide-Mediated Apoptosis in Human Cancer Cells. *Journal of Pharmacology and Experimental Therapeutics* **2010**, *334* (3), 710. DOI: 10.1124/jpet.110.167270.